Excitonically coupled cyanine dye dimers as optical energy transfer relays on DNA templates

Journal:	*ACS Applied Optical Materials*
Manuscript ID	ot-2023-004597.R2
Manuscript Type:	Forum Article
Date Submitted by the Author:	16-Mar-2024
Complete List of Authors:	Díaz, Sebastián; US Naval Research Laboratory, Center for Biomolecular Science and Engineering Kim, Young; US Naval Research Laboratory, Computational Materials Science Cunningham, Paul; US Naval Research Laboratory, Mathur, Divita; Case Western Reserve University, Chemistry Medintz, Igor; US Naval Research Laboratory, Kellis, Donald; Boise State University, Yurke, Bernard; Boise State University, Micron School of Materials Science & Engineering/Department of Electrical & Computer Engineering Knowlton, William; Boise State University, Micron School of Materials Science & Engineering; Department of Electrical and Computer Engineering Melinger, Joseph; US Naval Research Laboratory, Electronics Science and Technology Division

Excitonically coupled cyanine dye dimers as optical energy transfer relays on DNA templates

Sebastián A. Díaz[1], Young C. Kim[2], Paul D. Cunningham[3], Divita Mathur[4], Igor L. Medintz[1], Donald L. Kellis[5], Bernard Yurke[5,6], William B. Knowlton[5,6], and Joseph S. Melinger[3]*

[1]Center for Bio/Molecular Science and Technology, Code 6900, U.S. Naval Research Laboratory, Washington, DC 20375, USA

[2]Materials Science and Technology, Code 6300, U.S. Naval Research Laboratory, Washington, DC 20375, USA

[3]Electronics Science and Technology Division, Code 6800, U.S. Naval Research Laboratory, Washington, DC 20375, USA

[4]Department of Chemistry, Case Western Reserve University, Cleveland, OH, 44106

[5]Micron School of Materials Science & Engineering, Boise State University, Boise, Idaho 83725

[6]Department of Electrical and Computer Engineering, Boise State University, Boise, Idaho 83725

*Corresponding e-mail: joseph.melinger@nrl.navy.mil

KEYWORDS: Electronic energy transfer, FRET, Excitons, DNA nanotechnology, DNA scaffolds, Molecular photonic wires

ABSTRACT. An attractive strategy to improve the energy transfer properties of synthetic dye networks is to optimize the excitonic coupling between the dyes to increase energy transfer rates. To explore this possibility, we investigate the use of J-like cyanine dye dimers (Cy3 and Cy5 dimers) on DNA duplexes as energy transfer relays in molecular photonic wires. This approach is based on using the collective emission dipole of a J-dimer to enhance the FRET rate between the dimer relay and a remote acceptor dye. Experimentally, we find that in room temperature aqueous buffer conditions the dimer relay provided no benefit in energy transfer quantum yield relative to a simple monomer relay. Further investigation led us to determine that enhanced non-radiative relaxation, non-ideal dye orientation within the dimer, and unfavorable dye orientation between the dimer and the acceptor dye limit energy transfer through the dimer relay. We hypothesized that

non-radiative relaxation was the largest factor, and demonstrated this by placing the sample in a viscous solvent or cooling the sample, which dramatically improved energy transfer through the J-like dimer relay. Similar to how the formation of DNA-templated J-like dimers has improved, the practical use of J-like dimers to optimize energy transfer quantum efficiency will require improvements in the ability to control orientation between dyes to reach its full potential.

INTRODUCTION

Efficient electronic energy transfer (EET) in dye molecule networks is an essential property for applications in light harvesting,[1-3] organic solar cells,[4, 5] bio-sensing,[6] and exciton devices.[3, 7-12] While some applications only require a single efficient EET step, such as biosensors that use EET to signal the presence of an analyte,[13, 14] others require multiple EET steps to transfer energy over long distances, such as chemical sensing with conjugated polymers,[15] synthetic light harvesting antennae,[16-18] and molecular photonic wires (MPWs).[19-23] In order to improve the performance of synthetic molecular networks for efficient EET, it is necessary to optimize excitonic coupling between the constituent dye molecules to increase energy transfer rates.

In this work, we explore using J-like cyanine dimers as optical energy relays (hereafter, referred to simply as relays) to improve energy transfer quantum efficiency (EQE) in DNA

templated MPWs. We are motivated by the possibility that excitonically coupled chromophores can act collectively to enhance the rate of EET,[24, 25] which is a design principle used in natural light harvesting systems to achieve highly efficient EQE.[24]

In the dipole-dipole approximation the rate of EET can be written as,[26]

$$k_{EET} \propto \frac{\kappa^2 |\boldsymbol{\mu_D}|^2 |\boldsymbol{\mu_A}|^2}{R^6} J, \qquad \text{Eq. 1}$$

Where μ_D and μ_A are the transition dipole moments of the donor and acceptor, respectively, R is the center-to-center separation, J is the spectral overlap between the donor emission spectrum and the acceptor absorption spectrum, and κ is the orientation factor ($\kappa = (\hat{\mu}_D \cdot \hat{\mu}_A - 3(\hat{\mu}_D \cdot \hat{R}) \cdot (\hat{\mu}_A \cdot \hat{R}$)), where the circumflex indicates a unit vector). Consider the situation shown in **Figure 1a** where a pair of identical donor dyes is coupled to a monomer acceptor dye. If the donor dyes are arranged in a head-to-tail configuration of a so-called J-dimer ($\kappa = -2$), then the donor acts as a collective unit with an enhanced transition dipole of $\sqrt{2}\mu_D$.[24] In this case, **Equation 1** predicts a two-fold enhancement in k_{EET} when compared to the more common situation of two interacting monomers (assuming all other EET parameters remain the same). If both donor and acceptor are J-dimers, then a four-fold enhancement in EET is predicted.

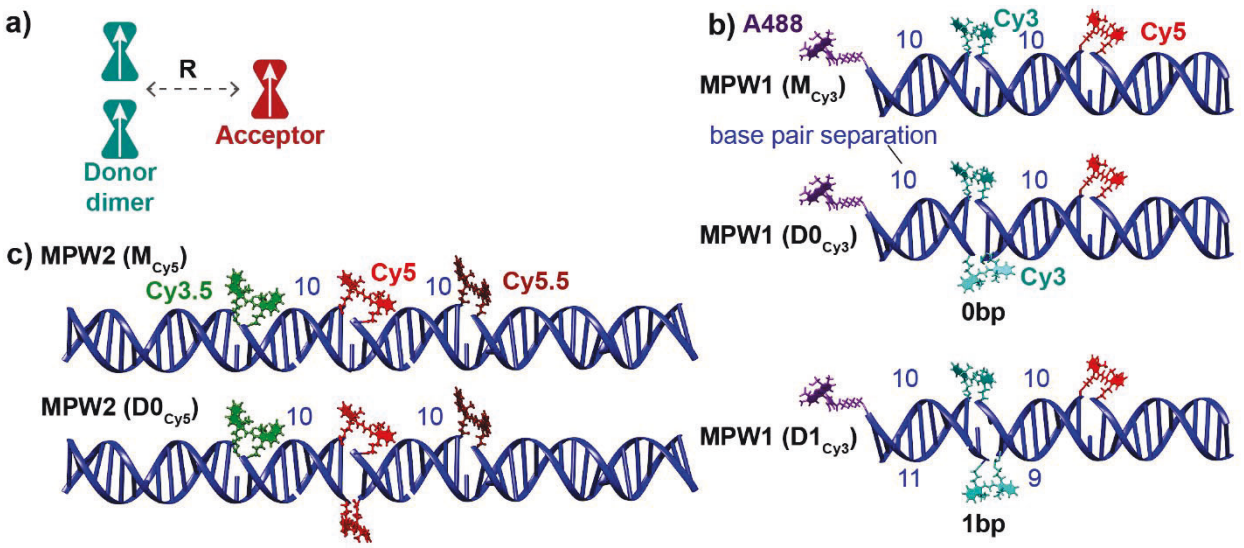

Figure 1. Dye-labeled DNA MPW structures utilized in this study. a) Schematic representation of an ideal J-dimer donor (green bowties) and a monomer acceptor (red bowtie) with a co-planar relative orientation, and with a center-to-center distance, *R*, between the J-dimer and the monomer. The white arrows inside the bowties represent the direction of transition dipole moments. b) and c) Schematic representations of molecular photonic wires (MPWs) using Cy3 (b) and Cy5 relay dyes (c). The Cy3 MPW consists of an initial A488 donor, Cy3 relay, and Cy5 terminal acceptor. The Cy5 MPW consists of an initial Cy3.5 donor, Cy5 relay, and Cy5.5 terminal acceptor. The separation between different dye types is given in base pairs (bp) between the attachment points of the dyes. The dimer relays $D0_{Cy3}$ and $D0_{Cy5}$ have Cy3 and Cy5 pairs attached at the same location along the DNA duplex, so-called 0 bp dimers. The dimer relay $D1_{Cy3}$ has Cy3 pairs separated by 1 bp along the DNA duplex, so-called 1 bp dimer.

In the context of DNA scaffolding, many strongly coupled dye dimers covalently attached to DNA have shown the characteristics of H-dimers, where the dyes are orientated co-facially (

$\kappa = 1$), and which exhibit blue-shifted absorption spectra compared to the monomer, and weak fluorescence.[27-30] Using an H-dimer as the donor would suppress k_{EET} because the lowest excitonic state of an ideal H-dimer carries no oscillator strength, though an H-dimer could be used as an acceptor to boost k_{EET}. However, beginning with the work of Häner and co-workers,[31] several examples of Cy3 and Cy5 dimers templated on DNA have shown J-like characteristics,[29, 32-35] where the absorption spectra are red-shifted from the monomers. Theoretical modeling of these cyanine dimers has suggested that they are not ideal J-dimers, rather they are better described as oblique dimers that exhibit Davydov splitting.[29, 32, 34, 35] We seek to understand whether such Cy3 and Cy5 dimers, as approximations to ideal J-dimers, can result in improved energy transfer relays in MPWs.

To this end, we designed two MPWs that utilize either a Cy3 dimer or Cy5 dimer as a relay between single dye initial donors and acceptors. The Cy3 dimer design is denoted MPW1, while the Cy5 dimer design is referred to as MPW2. The purpose for using two MPWs is to test whether the coupling strength of the dimers (Cy5 > Cy3) modifies the energy transfer throughput. The complete set of controls were also tested, including 'no relay' and 'monomeric relay' designs.

We characterize the optical properties and EQEs of MPWs and control structures using steady state and time resolved spectroscopy. Energy transfer is interpreted using Förster theory within dynamic and static isotropic limits of dye orientation, as well as in the context of constrained dye orientation that is observed from molecular dynamics (MD) simulations. After initial characterization, viscosity alterations and temperature-dependent measurements allow us to determine underlying mechanisms limiting EQE. For both MPWs, we find that rapid non-radiative excited state relaxation of the dimer limits the EQE, and this is especially so for the more strongly coupled Cy5 dimer. We show that suppressing non-radiative relaxation by increasing viscosity, or by moderately cooling the sample, can dramatically improve EQE. In addition, in the case of MPW1, we perform MD simulations, which suggest that the Cy3 dimer relay and Cy5 acceptor are constrained in unfavorable orientations that limit the EQE.

MATERIALS AND METHODS

MPW design:

Figure 1b schematically represents the two MPWs (MPW1 and MPW2). The design uses a 32 base pair (bp) double-stranded DNA (dsDNA) scaffold with dye structures, DNA sequences, and dye placement on the DNA strands described in the Supporting Information (**SI**; **Figures S1**, **Schemes S1** and **S2**, and **Tables S1** and **S2**). Dye-labeled DNA strands were HPLC purified ensuring nearly 100% labeling efficiency of the oligonucleotide. For MPW1, Alexa 488 (A488) is the donor, Cy3 monomer or dimer is the relay unit, and Cy5 is the acceptor. The three relay variants include a monomer (M_{Cy3}), a so-called 0 bp Cy3 dimer ($D0_{Cy3}$), and a so-called 1 bp Cy3 dimer ($D1_{Cy3}$). For $D0_{Cy3}$, one Cy3 dye is attached to each DNA strand at the same position along the DNA base stack positioning them directly opposite each other in the ds structure (**Scheme S1**). For $D1_{Cy3}$, the two Cy3 dyes are separated along the DNA base stack by one bp (**Scheme S1**). Cy3 and Cy5 are doubly attached to DNA using a three-carbon linker, whereas A488 is attached to the 5' end of a DNA strand using a flexible single-point linker (**Figure S1**). The three fully labeled MPW1s are called MPW1(M_{Cy3}), MPW1($D0_{Cy3}$), and MPW1($D1_{Cy3}$). MPW2 uses Cy3.5 as the donor, Cy5.5 as the acceptor, and two different relays: a Cy5 monomer, M_{Cy5}, and a 0 bp Cy5 dimer, $D0_{Cy5}$. All of the

dyes in MPW2 are doubly attached using three-carbon linkers. For MPW2, an important distinction is its modular design (**Scheme S2**) that uses four DNA strands to form the DNA duplex. This design was used to mitigate the high cost and low synthetic yield of DNA strands labeled with three dyes. In addition to fully labeled MPWs, we also assembled partially labeled control structures (C) from the DNA strands in **Tables S1** and **S2**. The control structures are used to help understand the individual energy transfer steps in the fully labeled MPWs, and to determine EQEs.

Sample Preparation: DNA duplexes were formed at 2 μM by heating the complementary strands to 94 °C and then ramping the temperature down to 4 °C, using a ramp with a 1 °C decrease every 30 second ramp. All experiments were performed in 2.5× phosphate buffered saline (0.345 M NaCl; 0.00675 M KCl; pH 7.4; henceforth referred to as PBS), and in a 2:1 glycerol:H_2O mixture at 2.5× PBS after mixing with glycerol (henceforth referred to as Gly-PBS). The increase in solvent viscosity by addition of glycerol has been shown to suppress photo-isomerization in cyanine dyes, thereby leading to increased fluorescence quantum yields (QYs).[32, 36]

Absorption and Fluorescence: Steady-state absorption spectra at room temperature were measured for 110 μL samples at concentration between 1-2 μM in a 1 cm path length cuvette using an Agilent 8453 diode array UV-vis spectrophotometer. Fluorescence emission spectra at a concentration of

$\lesssim$ 1 μM and with a peak optical density less than 0.1 were measured using a Multifunction Microtiter Plate Reader (Tecan Infinite MR 1000 Pro) in a 96 well plate using 50 μL of sample with excitation at 466, 515, and 600 nm for excitation of A488, Cy3/Cy3.5, and Cy5/Cy5.5 dyes, respectively. Temperature-dependent fluorescence measurements (down to 170 K) were performed using a Fluoromax 3 spectrofluorometer (Horiba). The samples in Gly-PBS were loaded in a 1 cm path length cryogenic quartz cell (Firefly Sci) and mounted in a Janis STVP-100 sample-in-vapor cryostat. The sample concentration for the fluorescence measurements was 0.20 μM in ds DNA to keep the peak optical density below 0.1. All fluorescence emission spectra were corrected for instrumental effects.

Fluorescence Quantum Yields: QYs were measured at room temperature using a Fluoromax 3 spectrofluorometer (Horiba) with an orthogonal excitation/detection geometry, and using known standards: Fluorescein, Rhodamine B, Cresyl Violet for A488, Cy3, and Cy5, respectively. The solutions were diluted so that peak optical densities were < 0.1 to ensure a uniformly excited volume and the linearity of the fluorescence emission spectra with concentration was confirmed to rule-out inner-filter effects.[37] The A488 fluorescence intensity was referenced to Fluorescein in basic ethanol (QY = 0.92),[38] Cy3 was referenced to Rhodamine B in ethanol (QY = 0.68),[39] Cy3.5

was referenced to Sulforhodamine 101 in ethanol (QY = 0.90),[40] Cy5 was referenced to Cresyl Violet in ethanol (QY = 0.58),[41] and Cy5.5 was referenced to Rhodamine 800 in ethanol (QY = 0.25).[41]

Circular Dichroism Spectra: Circular dichroism measurements (CD) at room temperature were performed using a JASCO J-1500 CD spectrophotometer. Measurements were performed within the spectral range of 200-850 nm, with 1 nm step intervals, at 100 nm/min, four second digital integration time, at room temperature. CD spectra were measured using a sample concentration of 2μM in a 1 cm path length quartz spectrophotometer cell.

Fluorescence Lifetimes: The fluorescence lifetimes were measured at room temperature using time-correlated single photon counting (TCSPC). The excitation source was an 80 MHz, 7 ps pulse, 532 nm, frequency-doubled diode-pumped Nd:YVO4 laser (High-Q picoTRAIN). The dye-DNA structures were placed in a 1 mm path quartz spectrophotometric cell at a concentration between 1-2 μM. Sample fluorescence was collected and sent through a polarizer set to the magic angle and then filtered using a monochromator. A micro channel plate photomultiplier tube (Hamamatsu) was used to detect the fluorescence with a ~40 ps instrument response function. The TCSPC waveforms were collected with greater than 10,000 counts in the peak channel.

Energy Transfer Measurements: Sensitized acceptor fluorescence was used as the primary method for determining the end-to-end (*ee*) energy transfer quantum efficiency ($E_{ee,sens}$) of the MPWs. Sensitized fluorescence determines $E_{ee,sens}$ by quantifying the number of photons emitted by the terminal dye per number of photons absorbed by the donor,[42, 43]

$$E_{ee,sens} = \left(\frac{(\mathrm{F}_{MPW} - \mathrm{F}_C)}{F_D}\right)\left(\frac{QY_D}{QY_A}\right) \quad \text{Eq. 2}$$

where F_{MPW} is the integrated fluorescence spectrum of the acceptor in the fully labeled MPW, F_C is the integrated fluorescence of the control structure without the donor dye, which accounts for fluorescence that does not come from exciting the donor dye, and F_D is the integrated fluorescence from the donor-alone structure. QY_D and QY_A are the fluorescence quantum yields of the donor dye and the terminal acceptor dye, respectively.

We also use a second method to evaluate EQE for MPW1s based on measuring steady state donor fluorescence quenching (also called donor loss) within donor-acceptor pairs,

$$E_{DL} = 1 - \frac{F_{DA}}{F_D}, \quad \text{Eq. 3}$$

where F_{DA} is the integrated fluorescence from the donor in the presence of the acceptor, and F_D is the integrated fluorescence from the donor alone. Using donor loss measurements, the end-to-end

EQE ($E_{ee,DL}$) of the MPWs are estimated by considering the energy transfer to be a two-step sequential process,[44]

$$E_{ee,DL} = E_{12} \times E_{23} \,, \qquad \text{Eq. 4}$$

where E_{12} is the EQE of the first step, E_{23} is the EQE of the second step, and labels 1, 2, and 3 represent the donor, relay, and acceptor dyes of the MPWs, respectively. We note that **Equation 4** ignores the direct energy transfer from the first donor to the terminal acceptor, however for the MPWs direct energy transfer is relatively small.[45]

Förster Resonance Energy Transfer (FRET) Analysis. For each dye pair, the Förster distance (R_0) corresponding to the donor-acceptor distance resulting in 50% EQE was determined using the equation,[46]

$$R_0^6 = 8.8 \times 10^{23} \frac{\kappa^2 Q Y_D}{n^4} J \,, \qquad \text{Eq. 5}$$

where QY_D is the fluorescence quantum yield of the donor in the absence of the acceptor, n is taken to be the refractive index of the solvent (n = 1.33 for the aqueous buffer, and n = 1.43 for the glycerol buffer), $\kappa^2$is the dipole orientation factor,[46] and J is the spectral overlap integral, given by[46]

$$J = \int_0^{\infty} \frac{\varepsilon_A(\upsilon) f_D(\upsilon)}{\upsilon^4} d\upsilon, \quad \text{Eq. 6}$$

where $f_D(\upsilon)$ is the fluorescence spectrum of the donor normalized to 1, $\varepsilon_A(\upsilon)$ is the molar absorptivity spectrum of the acceptor, and υ is the frequency in wavenumbers. We determined the theoretical EQEs between individual donor-acceptor pairs using the equation,

$$EQE = \frac{R_0^6}{R_0^6 + R^6} \ , \quad \text{Eq. 7}$$

where R is the center-center separation between the donor dye and the acceptor dye. Alternatively, **Equation 7** can be written in terms of rate constants,

$$EQE = \frac{k_{FRET}}{k_{tot} + k_{FRET}} \quad \text{Eq. 8}$$

where k_{FRET} is the rate constant for FRET and k_{tot} is the total relaxation rate constant from the excited state, equal to the sum of radiative and non-radiative relaxation rates of the donor dye in the absence of the acceptor.

Molecular Dynamics Simulation: MD simulations were carried out with the Gromacs 5.1.5 package[47] using Amber OL 15 force field parameters[48] for DNA and the general Amber force field (GAFF)[49] for dyes. The long-range electrostatics were computed using the particle-mesh Ewald

method with a real-space Coulomb cutoff of 1.0 nm. The van der Waals interactions were cut off at 1.0 nm. All bonds were constrained using the LINCS algorithm.[50] The neighbor searching algorithm was used with a cutoff of 1.0 nm, and the neighbor list was updated every 10th step. A time step of 2 fs was used for all simulations. The starting dye–DNA structures were built using the UCSF Chimera software, production version 1.13.1.[51] Rectangular periodic boundary conditions were used with the box dimensions of ~13.5 nm × 13.5 nm × 13.5 nm, ensuring a water layer of at least 1 nm between the DNA and the edge of the box. The systems were solvated in TIP3P water, and Na^+ and Cl^- ions were added to satisfy the salt concentration of 350 mM. The systems were then energy-minimized using the steepest descent method for 1000 steps. The systems were first equilibrated for 10 ns at a constant temperature of 300 K and pressure of 1 atm. The dye–DNA and solvent were coupled separately to temperature baths of the reference temperature (300 K) with a coupling time of 0.1 ps, whereas the pressure was kept constant to a bath of the reference pressure (1 atm) using a coupling time of 1.0 ps. The production trajectories of the dye-DNA complex were calculated for 1 μs, keeping the number of particles, temperature, and pressure constant. The Langevin thermostat[52] was used at 300 K with a coupling constant of 1 ps applied to dye–DNA and water separately. The pressure was maintained at 1 atm isotropically

with the Parrinello–Rahman barostat[53] and a coupling constant of 2.0 ps. The coordinates were written every 100 ps for the analysis.

RESULTS AND DISCUSSION

Structural and photophysical characterizations were undertaken to provide context to the EET analysis. A 20% polyacrylamide gel electrophoresis (PAGE) determined that the formation efficiency of MPW1 and MPW2 was dye and design independent, and greater than 90% in each case (**Figure S2**) - we note that we have observed that for simple DNA nanostructures PAGE underestimates solution level formation percentages.[54] Our samples typically showed high reproducibility in their optical spectra. As an example, sample batches prepared under the same conditions over 3-4 years (**Figure S3**) show highly reproducible absorption and fluorescence spectra. In addition, dilution assays showed that the formation efficiency was not modified over an order of magnitude around the 2 μM target concentration (**Figure S3**). DNA melting temperatures ranged from 35-75 ˚C, assuring well-formed structures at the buffer and working temperature (20 ˚C). We also determined the photophysical properties including the fluorescence QY for each dye (**Table 1**), and calculated the Förster radius, R_0, for each dye pair using the value for the dynamically averaged orientation factor, $\kappa^2 = 2/3$ (**Table 2**). For this analysis, we considered the coupled Cy3 and Cy5 dimers as a single donor/acceptor unit. We assume that the distances between donor and relay, and relay and acceptor ($\gtrsim$ 36 Å) are large enough so that EET can be

described by FRET. When the dimer acts as an acceptor, R_0 tends to increase with respect to the monomer acceptor because of the increase in the density of acceptor states, while changes in QY changes mean that dimers acting as donors can have either higher or lower efficiency than monomers.

Table 1. Fluorescence quantum yields of dye monomers and dye dimers.

Solvent	A488	M_{Cy3}	$D0_{Cy3}$	$D1_{Cy3}$	Cy3.5	M_{Cy5}	$D0_{Cy5}$	Cy5.5
PBS	0.74±0.04	0.28±0.04	0.16±0.04	0.23±0.03	0.31±0.02	0.33±0.04	0.04±0.01	0.24±0.04
Gly-PBS	0.81±0.05	0.64±0.04	0.68±0.07	0.47±0.06	0.51±0.02	0.41±0.04	0.20±0.02	0.33±0.05

The uncertainty is the standard deviation of three measurements.

Table 2. Spectral overlaps (J) and Forster radii (R_0) for MPW1 FRET pairs.

Structure/Solvent	J(cm^6/mmol)	R_0 (Å)*
A488-M_{Cy3} PBS	5.57×10^{-13}	65±1
A488-M_{Cy3} Gly	5.45×10^{-13}	63±1
A488-$D0_{Cy3}$ PBS	12.0×10^{-13}	74±1
A488-$D0_{Cy3}$ Gly	11.7×10^{-13}	72±1
A488-$D1_{Cy3}$ PBS	11.9×10^{-13}	74±1
A488-$D1_{Cy3}$ Gly	11.7×10^{-13}	72±1
M_{Cy3}-Cy5 PBS	8.36×10^{-13}	59±2
M_{Cy3}-Cy5 Gly	8.60×10^{-13}	65±1
$D0_{Cy3}$-Cy5 PBS	9.27×10^{-13}	55±2
$D0_{Cy3}$-Cy5 Gly	9.15×10^{-13}	66±1
$D1_{Cy3}$-Cy5 PBS	9.45×10^{-13}	59±2
$D1_{Cy3}$-Cy5 Gly	9.72×10^{-13}	63±1

* The values for R_0 are calculated using $\kappa^2 = 2/3$. The uncertainty in R_0 is calculated from the uncertainty in fluorescence quantum yields

MPWs with Cy3 relays.

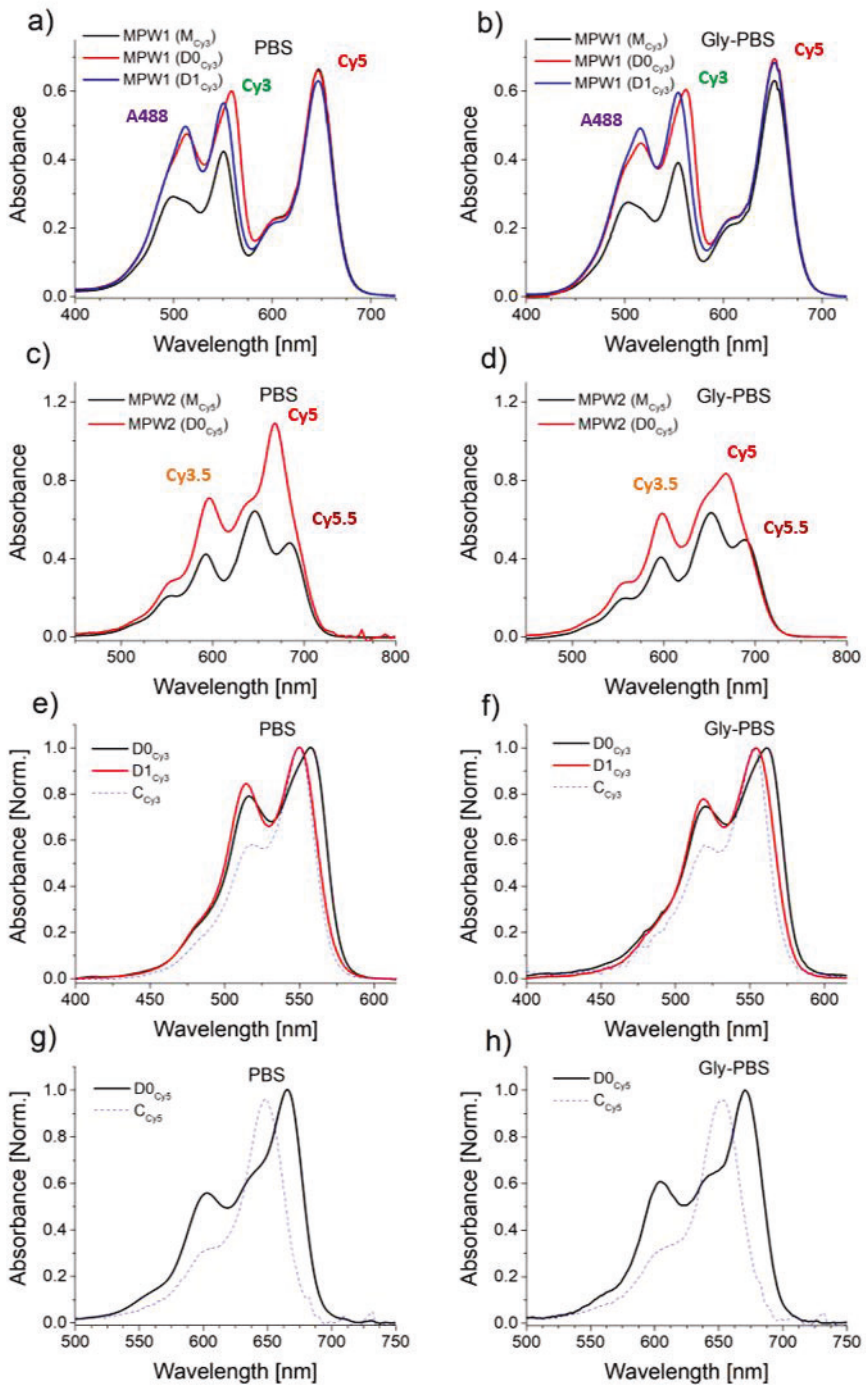

Figure 2. Absorption spectra for MPWs in PBS and Gly-PBS at room temperature. Panels a) and b) show absorption spectra for MPW1(M_{Cy3}) (black curve), MPW1($D0_{Cy3}$) (red curve), and

MPW1($D1_{Cy3}$) (blue curve). Panels c) and d) show absorption spectra for MPW2(M_{Cy5}) (black curve) and MPW2($D0_{Cy5}$) (red curve). The approximate absorption maxima for each dye is indicated. Panels e) and f) show absorption spectra for $D0_{Cy3}$ in PBS and Gly-PBS, respectively. Panels g) and h) show absorption spectra for $D0_{Cy5}$ in PBS and Gly-PBS, respectively. The blue dotted lines are the corresponding monomer absorption spectrum.

Figures 2a and 2b show absorption spectra of the MPW1s in PBS and Gly-PBS. Each case shows absorption peaks due to A488, Cy3, and Cy5 near 500 nm, 550 nm, and 650 nm, respectively. A notable feature is the increased absorption in the 550 nm region from the Cy3 dimer, and in the A488 region from the overlap of the vibronic bands of the Cy3 dimer with the peak of the A488 absorption. For MPW1($D0_{Cy3}$), there is a red shift of the absorption peak in the Cy3 region, which is suggestive of coupled Cy3 dyes in a J-like configuration. The differences in the absorption band shapes for the Cy3 monomer and dimers are shown in **Figures 2e and 2f** and **Figure S4**. With respect to Cy3, the absorption peak of $D0_{Cy3}$ is red-shifted by approximately 9 nm and the vibronic absorption band near 515 nm is enhanced with respect to the Cy3 monomer. The size of the red shift suggests a Davydov splitting of about 500 cm^{-1} (i.e., twice the red shift), which is consistent with previous J-like Cy3 dimers that we have studied.[32] In contrast, the $D1_{Cy3}$ does not show a red-shifted peak absorption, however the vibronic peak is enhanced with respect to

Cy3.[32] This result shows that the Cy3 dyes in $D1_{Cy3}$ are more weakly coupled. The CD spectrum for $D0_{Cy3}$ (**Figure S5**) shows a bisignate signal, confirming an excitonically coupled dimer. In contrast, the CD signal for $D1_{Cy3}$ is barely resolvable from the noise floor, which is consistent with much weaker coupling.

To quantify end-to-end energy transfer quantum yields ($E_{ee,sens}$), we performed steady-state fluorescence measurements while preferentially exciting the A488 donor dye at 466 nm (**Figure 3**). The fluorescence in the A488 region is highly quenched in all MPW1s with MPW1($D0_{Cy3}$) and MPW1($D1_{Cy3}$) showing stronger quenching than MPW1(M_{Cy3}). This result is consistent with the increased molar absorptivity of $D0_{Cy3}$, which leads to an increase in R_0 for the A488 → $D0_{Cy3}$ ($D1_{Cy3}$) FRET step. Interestingly, quenching of A488 fluorescence in Gly-PBS is smaller than in PBS. A possible explanation is that interactions between A488 and the DNA duplex are weaker in Gly-PBS, which would allow the end attached A488 to move farther away from the DNA duplex and increasing its distance from the downstream acceptor dyes. The terminal Cy5 fluorescence of the MPW1s show different relative intensities in PBS and Gly-PBS. In PBS, the Cy5 fluorescence intensity for MPW1($D0_{Cy3}$) is similar to MPW1(M_{Cy3}), with both being lower than MPW1($D1_{Cy3}$). In Gly-PBS, both MPW1($D0_{Cy3}$) and MPW1($D1_{Cy3}$) show similar fluorescence intensity from

Cy5, with MPW1(M_{Cy3}) showing lower Cy5 fluorescence intensity. The MPW1 fluorescence spectra are decomposed into linear combinations of component spectra (**Figure S6**) while accounting for direct excitation of the downstream dyes. The $E_{ee,sens}$ values (**Table 3**) for MPW1s were then determined using **Equation 2**. To calculate the theoretical $E_{ee,dyn}$ for the MPW1s, we used R = 36 Å (10 bp separation at 3.6 Å/bp)[55] in **Equation 7** to estimate the distance between the Cy3 donors and the Cy5 acceptor, and R = 40 Å to estimate the distance between the A488 donor and the Cy3 monomer and dimer acceptors, where the extra 4 Å is used to account for the flexible linker of the A488 donor. The R_0 values in **Table 2** were used in **Equation 7**.

Table 3. Experimental and theoretical end-to-end energy transfer quantum efficiencies from fluorescence measurements at room temperature.

Structure/Solvent	Experimental		Theoretical	
	$E_{ee,sens}$*	$E_{ee,DL}$**	$E_{ee,dyn}$***	$E_{ee,stat}$
MPW1(M_{Cy3}) PBS	0.52 ± 0.11	0.68	0.90	0.62
MPW1(M_{Cy3}) Gly-PBS	0.57 ± 0.18	0.66	0.93	0.66
MPW1($D0_{Cy3}$) PBS	0.36 ± 0.08	0.45	0.90	0.65
MPW1($D0_{Cy3}$) Gly-PBS	0.56 ± 0.24	0.65	0.96	0.72
MPW1($D1_{Cy3}$) PBS	0.53 ± 0.12	0.75	0.93	0.69
MPW1($D1_{Cy3}$) Gly-PBS	0.56 ± 0.22	0.74	0.95	0.71
MPW2($D0_{Cy5}$) PBS	0.10 ± 0.04	-	0.69	0.42
MPW2($D0_{Cy5}$) Gly-PBS	0.57 ± 0.16	-	0.69	-

* Uncertainty is determined from the standard deviation of three measurements.

** $E_{ee,DL}$ is determined from a single measurement. An uncertainty of ± 5% is assumed.

***The average value of R_0 from Table 2 is used to compute the value of $E_{ee,dyn}$.

"*dyn*" means dynamic averaging limit; "*stat*" means static isotropic limit.

Blank entries mean the quantity was not measured/calculated.

Equation 9 is used to calculate $E_{ee,stat}$.

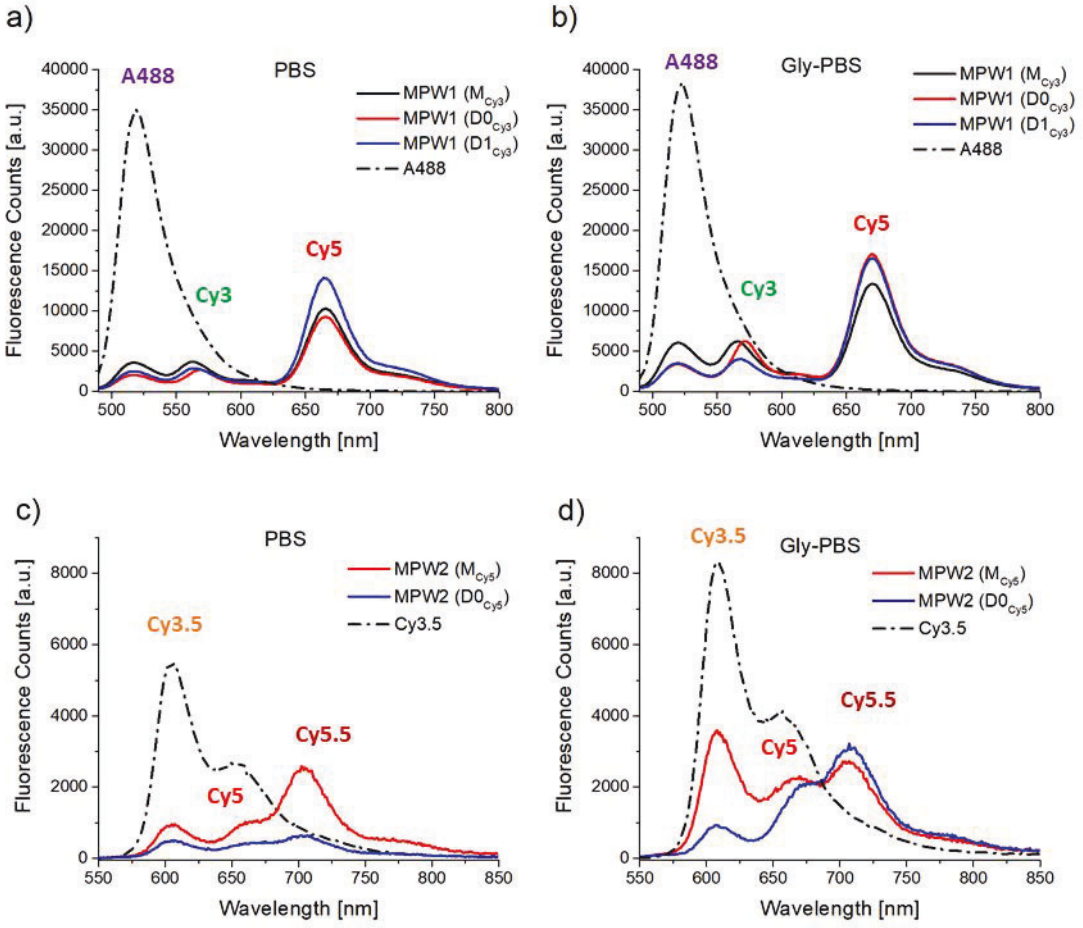

Figure 3. Steady state fluorescence spectra for MPWs in PBS and Gly-PBS at room temperature.

Panels a) and b) show fluorescence spectra of MPW1(M_{Cy3}) (black curve), MPW1($D0_{Cy3}$) (red curve), and MPW1($D1_{Cy3}$) (blue curve). The dotted black line is the fluorescence spectrum from the A488 donor-only control structure, C_{A488}. The excitation wavelength for MPW1s is 466 nm. Panels c) and d) show fluorescence spectra of MPW2(M_{Cy5}) (black curve) and MPW2($D0_{Cy5}$) (red curve). The dotted black curve is the fluorescence spectrum from the Cy3.5 donor-only control

structure, $C_{Cy3.5}$. The excitation wavelength for MPW2s is 515 nm. Approximate fluorescence maxima for each dye is indicated.

In PBS, $E_{ee,sens}$ for MPW1($D0_{Cy3}$) is 0.36 ± 0.08 and substantially lower than for both MPW1(M_{Cy3}) (0.52 ± 0.11), and MPW1($D1_{Cy3}$) (0.53 ± 0.12). In Gly-PBS, $E_{ee,sens,}$ for MPW1($D0_{Cy3}$) increases by 55% to 0.56 ± 0.24, reaching the same efficiency as MPW1(M_{Cy3}) and MPW1($D1_{Cy3}$). This result is counter to expectations; theoretical predictions based on R_0 values (**Table 2**) would predict that the $D0_{Cy3}$ and $D1_{Cy3}$ relays should be at least as efficient, if not more efficient, than the M_{Cy3} relay. Two hypotheses can be drawn from this initial data set. The first is that the non-radiative decay pathways created by the Cy3 dimerization have a larger impact on the EQE than the increase in transition dipole, leading to a net decrease. This hypothesis is supported by the substantial increase in EQE when in Gly-PBS. We note that the increase in EQE is accompanied by a four-fold increase in the fluorescence QY of $D0_{Cy3}$ in Gly-PBS (**Table 1**), and an associated increase in R_0 (**Table 2**).

To gain additional insight, we performed fluorescence lifetime measurements of the Cy3 relays in PBS and Gly-PBS (**Figure 4**). The average lifetime ($\langle\tau\rangle$) of each curve was determined from multi-exponential fits (**Table S3**). For each relay, the average fluorescence lifetime increased in Gly-PBS, with $D0_{Cy3}$ showing the largest increase consisting of a factor of 2.5. In the **SI** (**Section 6**), we calculate the non-radiative rate constants (k_{nr}) for Cy3 and $D0_{Cy3}$ relays in PBS and Gly-

PBS (**Table S4**) using $\langle\tau\rangle$ and the fluorescence QYs in **Table 1**. In PBS, k_{nr} for $D0_{Cy3}$ (2.1×10^9

s^{-1}) is $\sim 3.2\times$ larger than k_{nr} for Cy3 ($0.67 \times 10^{9} s^{-1}$). This result is consistent with the lower

EQE for MPW($D0_{Cy3}$) in PBS. In Gly-PBS, k_{nr} for $D0_{Cy3}$ ($0.21 \times 10^9 s^{-1}$) is highly suppressed compared to PBS and is only slightly larger than k_{nr} for Cy3 ($0.18 \times 10^9 s^{-1}$). This is consistent with the similar EQEs for MPW1(Cy3) and MPW($D0_{Cy3}$) in Gly-PBS. Increased fluorescence lifetimes of Cy3 monomers in viscous environments has been attributed to suppression of

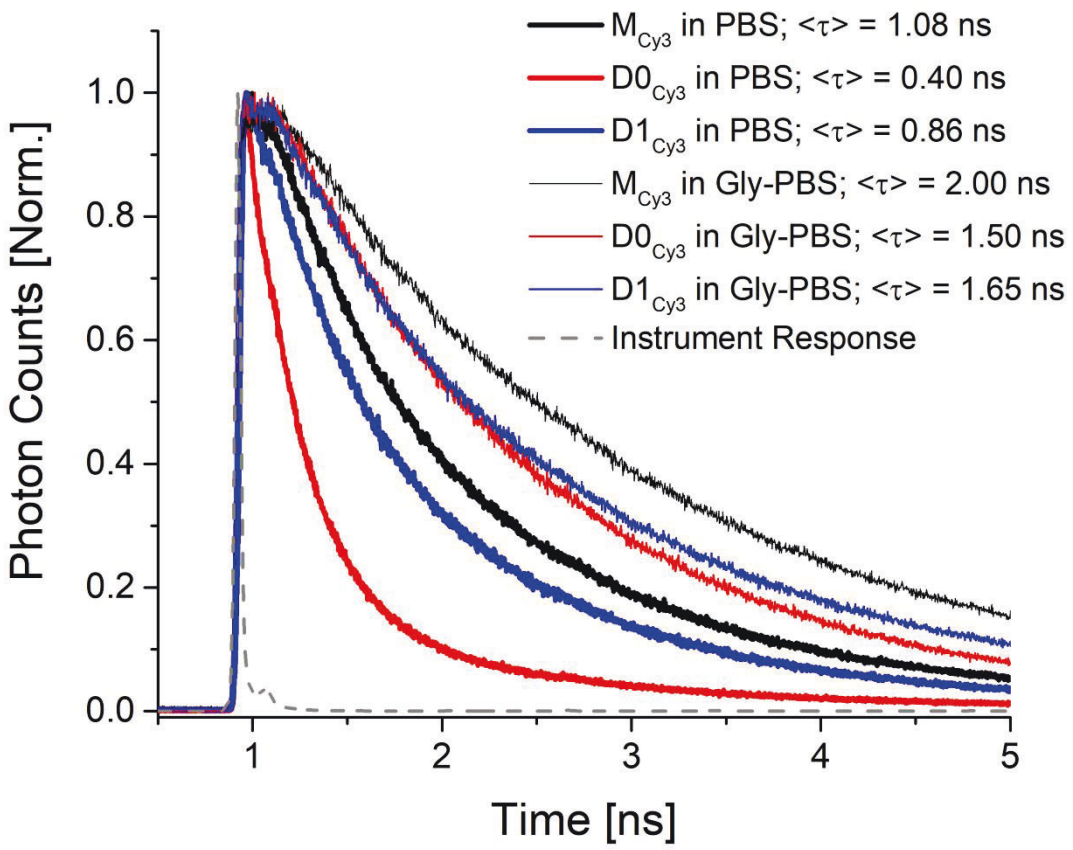

photoisomerization.[32, 36] While the exact mechanism for the increased fluorescence lifetime of $D0_{Cy3}$ in Gly-PBS is not yet established, we can conclude that the increase in the EQE of MPW1($D0_{Cy3}$) is due to suppression of non-radiative relaxation in $D0_{Cy3}$.

Figure 4. Fluorescence decay curves measured by TCSPC at room temperature for DNA duplexes containing Cy3 monomers or dimers. Fluorescence decay curves measured by TCSPC at room temperature for DNA duplexes containing Cy3 monomers or dimers. The thick solid curves are fluorescence decays measured in PBS and the thin solid curves are fluorescence decays measured in Gly-PBS. The gray dashed line is the instrument response. The average fluorescence lifetime, $<\tau>$, for each construct is shown in the legend.

Using the fluorescence lifetimes in **Table S3** and **Equation 8**, we estimate the FRET rate constants (k_{FRET}) for the $D0_{Cy3} \rightarrow$ Cy5 and Cy3 → Cy5 steps. The calculation produces smaller k_{FRET} for $D0_{Cy3} \rightarrow$ Cy5 ($k_{FRET} = 2.31 \times 10^9 s^{-1}$in PBS; $k_{FRET} = 2.25 \times 10^9 s^{-1}$ in Gly-PBS) than for Cy3 → Cy5 ($k_{FRET} = 2.85 \times 10^9 s^{-1}$in PBS; $k_{FRET} = 2.40 \times 10^9 s^{-1}$ in Gly-PBS). This result is consistent with the lower energy transfer efficiency through the $D0_{Cy3}$ relay relative to the Cy3 monomer relay.

Theoretical considerations based on R_0 values (**Table 3**) predict that the $D0_{Cy3}$ and $D1_{Cy3}$ relays should be at least as efficient, if not more efficient, than the M_{Cy3} relay, while experimentally we find that $D0_{Cy3}$ is less efficient and see no difference for $D1_{Cy3}$ (based on $E_{ee,sens}$), even in Gly-PBS where we showed that non-radiative relaxation in the Cy3 dimer is suppressed. We therefore suggest a second hypothesis to more completely explain the lower than expected EQE of MPW1s, particularly MPW1($D0_{Cy3}$), which is that the dimers are not properly represented by the dynamic

averaging where κ^2 is be approximated by 2/3. As is discussed later in the manuscript, we believe that dimers result in lower κ^2 values that limit the EQE.

To test the second hypothesis, we evaluated the EQEs for MPW1s based on donor fluorescence quenching (**Equations 3** and **4**) using values of $E_{ee,DL}$ shown in **Table S5**. The trend in $E_{ee,DL}$ over the MPW1s shows qualitative agreement with $E_{ee,sens}$, though $E_{ee,DL}$ produced between 15-35% higher efficiency (**Table 3**). We note that a similar discrepancy between the donor loss and sensitized fluorescence methods in determining the EQE has been observed in other works.[44] One observation from **Table 3** and **Table S5** is that the experimental EQE values for each of the MPW1s are much lower than the theoretically predicted values in the dynamical averaging limit ($\kappa^2 = 2/3$). The large discrepancies between experimental and theoretical EQEs suggests that the dynamical averaging limit is not appropriate to interpret the experimental measurements.

We next determined whether the experimental results could be interpreted by using a static isotropic distribution of dye orientations (see **Figure S9**).[56, 57] In this limit, the dyes in the ensemble are considered to remain fixed during the FRET process and they can assume all possible dye orientations. The EQE is calculated by averaging **Equation 4** over an isotropic distribution of dipole orientation factors (κ^2), which results in,

$$E_{ee,stat} = \langle E_{12} \rangle \times \langle E_{23} \rangle = \sum_i \overline{P}_i E_{12,i} \times \sum_j \overline{P}_j E_{12,j} \, . \qquad \text{Eq. 9}$$

Equation 9 ignores contributions of direct energy transfer from donor to acceptor that do not involve the relay dyes. For example, the control structure $C_{A488\text{-}Cy5}$, lacking the intermediary Cy3 dye, has $E_{ee,sens}$ values of 0.068 ± 0.025 and 0.080 ± 0.024 in PBS and Gly-PBS, respectively, which are small compared to the values of the fully labeled MPW1s. Further, it has also been previously demonstrated that in linear arrays the direct transfer is further minimized in the presence of relay dyes.[45] **Equation 9** also ignores the possible dependences of the A488-$D0_{Cy3}$ spectral overlap and fluorescence QY of $D0_{Cy3}$ on the relative orientation of the Cy3 dyes. In principle, both of these factors can affect the EQE. Accounting for these effects requires a much more sophisticated theory than used here. In **Equation 9**, $\overline{P}_i$ represents the normalized isotropic distribution of dipole orientation factors, E_{12} represents the A488 → $D0_{Cy3}$ (Cy3) FRET step, and E_{23} represents the $D0_{Cy3}$ (Cy3) → Cy5 FRET step. The average was performed using Monte Carlo sampling of $\overline{P}_i$ (**Figure S9**).[56, 57] The results shown in **Table 3** generally show improved agreement with experimental EQE measurements. An outlier is MPW1($D0_{Cy3}$) in PBS where the discrepancy between the experimental and theoretical $E_{ee,stat}$ is 45%. The source of the relatively low experimental end-to-end EQE is from the relatively low FRET efficiency of the $D0_{Cy3}$ → Cy5 step

in PBS (**Table S5**). This observation suggests that, while the dyes might be static on the FRET timescale, the distribution of orientations may not be isotropic. We note evidence from experimental measurements[58-60] and molecular dynamics (MD)[58, 59] simulation that suggest that Cy3 and Cy5 dyes have constrained orientations when they are doubly attached to DNA origami scaffolds. For 0 bp Cy3 and Cy5 dimers on DNA duplexes, theoretical modeling of experimental optical spectra[34] and MD simulation[32, 61] suggest that the dyes assume a preferred distribution of orientations. In the context of this evidence, a plausible explanation for the relatively low energy transfer efficiency of MPW1($D0_{Cy3}$) is that the 0bp Cy3 dimer, and to a lesser extent the 1bp dimer, have unfavorable orientations with the Cy5 acceptor for high efficiency FRET.

Tables 3 and **S5** suggest that the $D0_{Cy3}$ → Cy5 FRET step is mainly responsible for the lower than anticipated EQE of MPW1($D0_{Cy3}$). To help understand whether unfavorable dye orientation is the reason for the low EQE of the $D0_{Cy3}$ → Cy5 FRET step, we performed MD simulations of MPW1($D0_{Cy3}$) and MPW1(M_{Cy3}) and focused on characterizing the fluctuations in κ^2 for the Cy3 monomers in $D0_{Cy3,}$ and in κ^2 for the $D0_{Cy3}$ – Cy5 pair. The results over one microsecond of MD simulation time are summarized in **Figure 5** and **Figures S10-S13**. The procedure for calculating the dipole orientation factors, inter-dye separations, and EQE from the

MD data is given in the **SI** (**Section 8**). **Figure 5a** shows a heat map of the intra-Cy3 κ^2 for the Cy3 dimer vs the center-to-center separation (r) between the Cy3 dyes. The heat map indicates that approximately 90% of the occurrences have a κ^2 value between 2 and 3 and with r between 11.5 and 14 Å. These are the most probable dimer configurations and they are best described as oblique dimers that are intercalated into the DNA base stack (e.g., **Figure S10a**). Within these configurations, the larger values of κ^2 correspond to larger oblique angles and Cy3 dimers that are closer to the ideal J-dimer. The heat map also shows minor occurrences near $\kappa^2 = 1$, which correspond to an H-like Cy3 dimer configuration. Finally, the heat map also shows minor occurrences near $\kappa^2 \sim 0$. It's not clear whether these configurations are monomer-like or strongly coupled because the dye separations are less than about 1 nm, which are smaller than the length of the Cy3 dye (~ 1.4 nm). Understanding this situation likely requires a numerical calculation using a vibronic exciton model.[29, 62, 63] A representative Cy3 dimer structure with an oblique angle of 115˚ and r = 12.5 Å is shown to the right of **Figure 5a**. **Figure 5b** shows a heat map of the dipole orientation factor between the Cy3 dimer and the Cy5 acceptor vs the center-to-center distance, R. Here, κ^2 is strongly biased to low values ($\kappa^2 < 0.5$), and R is centered near 40 Å. While the Cy3 dimer remains largely intercalated, we note that Cy5 assumes partially intercalated orientations

that result in values of κ^2 near zero, and non-intercalated orientations that result in larger values of κ^2. Representative configurations of $D0_{Cy3}$ and Cy5 on the DNA duplex are shown in **Figures 5b** and **S10b**. Fluctuations of the κ^2, R, and EQE are shown in **Figure S12**, from which the following ensemble averaged values of FRET quantities for the $D0_{Cy3}$ → Cy5 step are calculated: $\langle\kappa^2\rangle = 0.18$, $\langle R\rangle = 39$ Å, and <EQE> = 0.45 **(SI; Section 8)**, which is in good agreement with the experimental value from donor fluorescence quenching: $E_{DL} = 0.48$.

The results of the MD simulation for MPW1(M_{Cy3}) are shown in **Figure 5c**. The heat map shows that κ^2 varies between values near 0 and 1.1 and R varies between 30 – 40 Å. As above, from the fluctuations of the κ^2, R, and EQE (**Figure S13**), we calculate the ensemble averaged values of FRET quantities for the Cy3 – Cy5 step: $\langle\kappa^2\rangle = 0.63$, $\langle R\rangle = 35$ Å, and <EQE> = 0.89, which is somewhat higher than the experimental $E_{DL} = 0.76$ (**Table S5**). The ~ 2 × higher EQE for the Cy3 → Cy5 step is mainly due to the ~ 3.5 larger value of $\langle\kappa^2\rangle$. Both the Cy3 and Cy5 dyes in MPW1(M_{Cy3}) fluctuate between partly intercalated and non-intercalated configurations on DNA, which is responsible for the larger value of $\langle\kappa^2\rangle$. Overall, the reasonable agreements in EQE between experimental measurements and MD simulations support the hypothesis that unfavorable

relative orientations between D0Cy3 and Cy5 are responsible for the relatively low EQE of MPW1($D0_{Cy3}$).

Figure 5. Heat maps of the dipole orientation factor (κ^2) vs inter-dye center-to-center distances for MPW1($D0_{Cy3}$) and MPW1(M_{Cy3}). (a): Heat map for the Cy3 dimer ($D0_{Cy3}$). (b): Heat map for the $D0_{Cy3}$-Cy5 pair. (c): Heat map for the Cy3 – Cy5 pair. Representative MD snapshots for $D0_{Cy3}$

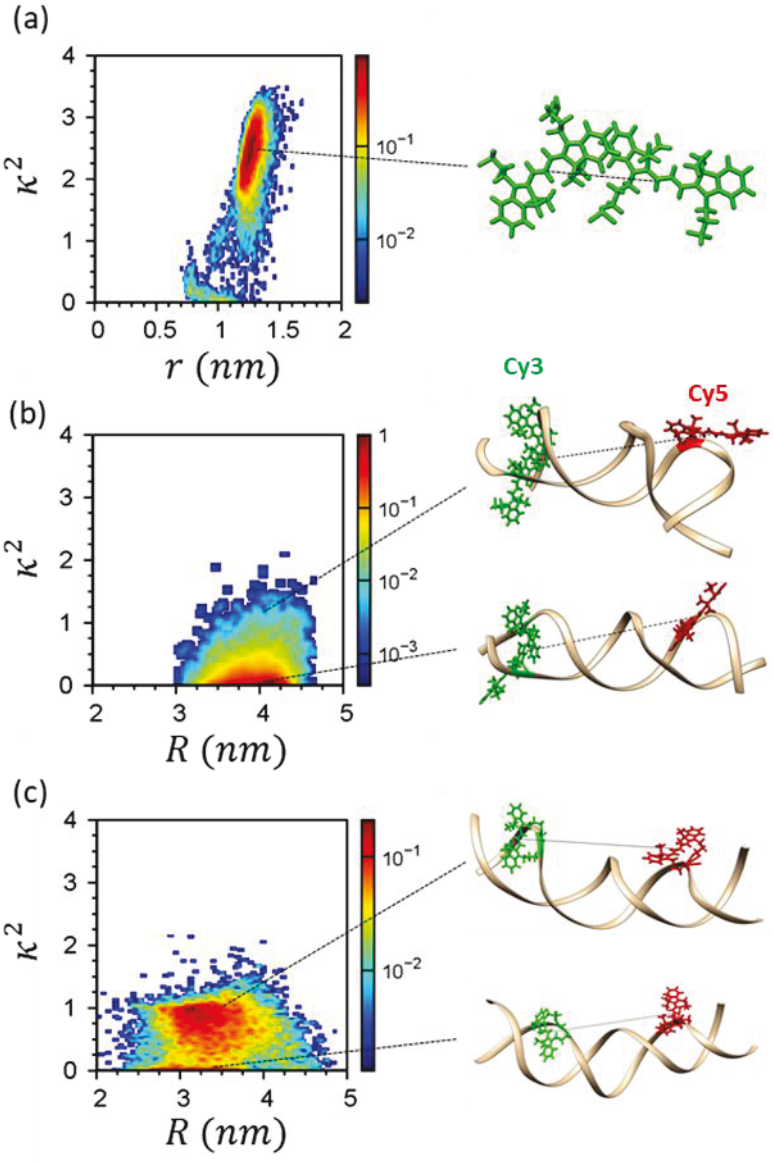

(DNA not shown), $D0_{Cy3}$ – Cy5, and Cy3 – Cy5 are shown to the right of each heat map. In (b), the structure on the top corresponds to κ^2 near 1 and is distinguished by a non-intercalated Cy5. The structure on the bottom corresponds to κ^2 near 0 and is distinguished by a partly intercalated Cy5. In (c), the structure on the top has both dyes in a near co-planar orientation. The structure on the bottom has the Cy3 partially intercalated and is nearly orthogonal to the non-intercalated Cy5. The color bars on the right indicate the normalized frequency of occurrence.

Even though we did not observe higher energy transfer efficiency through the Cy3 dimer relay compared to the Cy3 monomer relay, it is still useful to estimate the extent to which the Cy3 dyes in $D0_{Cy3}$ act as a collective unit. The size of exciton delocalization (N_{coh}) in the Cy3 dimer can be estimated from[64]

$$N_{coh} = \frac{QY_{dimer}\ \tau_{monomer}}{QY_{monomer}\ \tau_{dimer}} \qquad \text{Eq. 10}$$

where the QYs and fluorescence lifetimes of Cy3 and $D0_{Cy3}$ are used in **Equation 10**. Using values in **Table 1** and **Table S3,** $N_{coh} = 1.50 \pm 0.2$ for $D0_{Cy3}$ in PBS and $N_{coh} = 1.42 \pm 0.2$ for $D0_{Cy3}$ in Gly-PBS. A fully delocalized exciton in a dimer would achieve $N_{coh} = 2$,[62] thus we conclude that collective effects make a moderate contribution to the $D0_{Cy3} \rightarrow$ Cy5 FRET rate.

MPWs with Cy5 relays

We used Cy5 as the relay dye in a similar MPW system in order to test our initial conclusions and investigate energy transfer through a dimer relay with stronger excitonic coupling.

Cy5 has a larger transition dipole moment (~ 16 D)[61] and molar absorptivity (~ 250,000 $M^{-1}cm^{-1}$),[43] which makes it an excellent choice for creating strongly coupled dimers on DNA scaffolds. **Figures 2c** and **2d** show absorption spectra of MPW2s with M_{Cy5} and $D0_{Cy5}$ relays in PBS and Gly-PBS. In PBS, MPW2(M_{Cy5}) shows absorption peaks due to the Cy3.5 donor, the Cy5 monomer relay, and the terminal Cy5.5 acceptor near 590 nm, 630 nm, and 690 nm, respectively. In contrast, MPW2($D0_{Cy5}$) shows a relatively intense red-shifted peak near 667 nm indicative of strong J-like excitonic coupling, and a shoulder on the red edge of the absorption spectrum due to the peak of the Cy5.5 absorption spectrum. The absorption band shapes for C_{Cy5} and $D0_{Cy5}$ are shown in **Figure S4**. In PBS, with respect to C_{Cy5}, the low energy absorption of $D0_{Cy5}$ shows a clear Davydov splitting into two bands with a separation of approximately 33 nm, or about 780 cm^{-1}. In contrast, in Gly-PBS, the absorption band in the Cy5 region appears as a broadened peak (**Figure 2d**). Interestingly, the absorption spectrum of $D0_{Cy5}$ in Gly-PBS (without the donor and acceptor dyes), shows characteristic Davydov splitting (**Figure S4d**). These results suggest that in Gly-PBS, the presence of Cy3.5 and/or Cy5.5 destabilizes the modular DNA duplex, likely due to dye intercalations, producing a distribution of Cy5 dimer configurations. This appears true, even

though the melting temperature of the strand should be near 35 ˚C in our buffer conditions taking into account base stacking.[65]

CD spectra available in **Figure S5** provide additional insight into the stability of the modular DNA duplex. In PBS, the fully labeled MPW2($D0_{Cy5}$) and the control structures $D0_{Cy5}$ and $C_{D0_{Cy5}\text{-}Cy5.5}$ produce essentially the same CD spectra. In contrast, for MPW2($D0_{Cy5}$) in the Gly-PBS environment, the ~ 2 × weaker CD signal suggests that approximately half of the ensemble contains Cy5 dimers that have relaxed into monomer-like configurations with relatively larger separation between Cy5 dyes compared to $D0_{Cy5}$.

Figures 3c and 3d show steady-state fluorescence spectra for MPW2(M_{Cy5}), MPW2($D0_{Cy5}$), and the donor only control $C_{Cy3.5}$ in PBS and Gly-PBS when preferentially exciting Cy3.5 at 515 nm, and **Figure S7** shows the fluorescence spectra of the other control structures. In PBS, both MPW2s show strong quenching of Cy3.5 fluorescence. Stronger quenching of Cy3.5 fluorescence occurs in MPW2($D0_{Cy5}$), which is consistent with the presence of a second Cy5 dye increasing the density of final states of the acceptor. The most striking observation is the relatively low fluorescence intensity from the terminal Cy5.5 dye in MPW2($D0_{Cy5}$), which is 4-5 times

weaker than the Cy5.5 fluorescence from MPW2(M_{Cy5}). From **Equation 2**, $E_{ee,sens}$ is 0.53 ± 0.11 for MPW2(M_{Cy5}), but only 0.10 ± 0.04 for MPW2($D0_{Cy5}$) (**Table 3**). Considering the strong quenching of Cy3.5 fluorescence, the relatively low $E_{ee,sens}$ for MPW2($D0_{Cy5}$) is likely due to a low EQE for the $D0_{Cy5} \rightarrow$ Cy5.5 step. In contrast, in Gly-PBS the fraction of the total fluorescence that comes from the terminal Cy5.5 dye increases substantially for MPW2($D0_{Cy5}$) and $E_{ee,sens}$ increases to 0.57 ± 0.16. However, as described above, understanding the origin of the increased efficiency is complicated because the Cy5 dimer relay consists of a mixture of monomer-like species and coupled dimers. In the case of MPW2(M_{Cy5}) in PBS-Gly, $E_{ee,sens}$ actually decreases to 0.38 ± 0.10. The decrease in efficiency appears to be due to inefficient energy transfer from the Cy3.5 donor. This may be related to partial separation of the DNA strand containing Cy3.5 from the template strand, or DNA 'breathing' around that dye.

To better understand the low value of $E_{ee,sens}$ for MPW2($D0_{Cy5}$) in PBS, we compare the experimental result to the theoretical predictions in the dynamic and static isotropic limits. The estimation of R_0 is complicated by very weak fluorescence from the 0bp Cy5 dimer due to rapid picosecond timescale non-radiative relaxation at room temperature.[66] Thus, we refer to excited state lifetimes in the literature (τ) measured by ultrafast transient absorption measurements of

similar 0 bp Cy5 dimers ($\tau_{D0_{Cy5}}$ = 11 ps)[66] and Cy5 monomers (τ_{Cy5} = 1500 ps)[66] on DNA duplexes, from which we infer the fluorescence QY to be approximately 0.01. Using this value for the fluorescence QY in **Equation 7** results in R_0 ~ 4.1 nm for $D0_{Cy5}$ – Cy5.5. For MPW2($D0_{Cy5}$), the theoretical estimates for end-to-end EQE are 0.69 in the dynamic averaging limit, and 0.42 in the static isotropic limit (**Table 3**). Both of these theoretical estimates are much larger than the experimental $E_{ee,sens}$ = 0.10 ± 0.04. As with the case of MPW1($D0_{Cy3}$), a plausible explanation is that the dye orientations are static on the timescale of FRET, but are constrained in net orientations with low values of κ^2. The combination of rapid non-radiative relaxation and unfavorable dye orientation can account for the overall low EQE through the 0 bp Cy5 relay.

Instead of analyzing the individual energy transfer steps, as done for the MPW1s, we investigated whether we could increase EQE by suppressing rapid non-radiative excited state relaxation at lower temperatures. We measured temperature-dependent fluorescence emission spectra of MPW2($D0_{Cy5}$) and the controls $C_{Cy3.5}$, $C_{Cy5.5}$ and $C_{Cy5\text{-}Cy5.5}$ in Gly-PBS because the samples retain high optical quality until about 170 K, below which a solid glass forms producing increased light scattering. **Figures 6a** and **6b** show temperature-dependent fluorescence emission spectra and fluorescence excitation spectra for MPW2($D0_{Cy5}$). As the temperature is lowered the fluorescence emission bands narrow and the relative fluorescence intensity from Cy5.5 increases with respect to the residual fluorescence from Cy3.5 and $D0_{Cy5}$. Interestingly, just below room temperature at 270 K the fluorescence spectrum undergoes an abrupt transition. The $D0_{Cy5}$ fluorescence band (near 665 nm) red shifts and weakens in intensity with respect to the Cy5.5 fluorescence band (near 695 nm). A residual fluorescence band from Cy3.5 is observed near 600 nm. The fluorescence excitation spectrum (**Figure 6b**) also shows an abrupt transition at 270 K. The relatively broad band in the Cy5 region at 297 K has red shifted and evolved into two bands (near 635 nm and 667 nm) indicative of Davydov splitting. The Cy5.5 band is present in the excitation spectrum as a shoulder near 695 nm. These observations indicate that relatively

moderate cooling stabilizes the modular DNA duplex, and, as a consequence, favors formation of

the strongly coupled 0 bp Cy5 dimer relay. Further cooling to 170 K results in a relatively large

increase in terminal fluorescence from Cy5.5 and increased resolution of the two lowest excitonic

transitions of $D0_{Cy5}$ in the excitation spectrum. The gradual changes in the spectroscopic features

in the fluorescence emission and excitation spectra – gradual narrowing of the bands, gradual blue

shift the emission peaks, and gradual resolution of the Cy5 dimer Davydov splitting (**Figure 6B**) –

are consistent with the DNA duplex remaining stable as the temperature is lowered from 270 K to

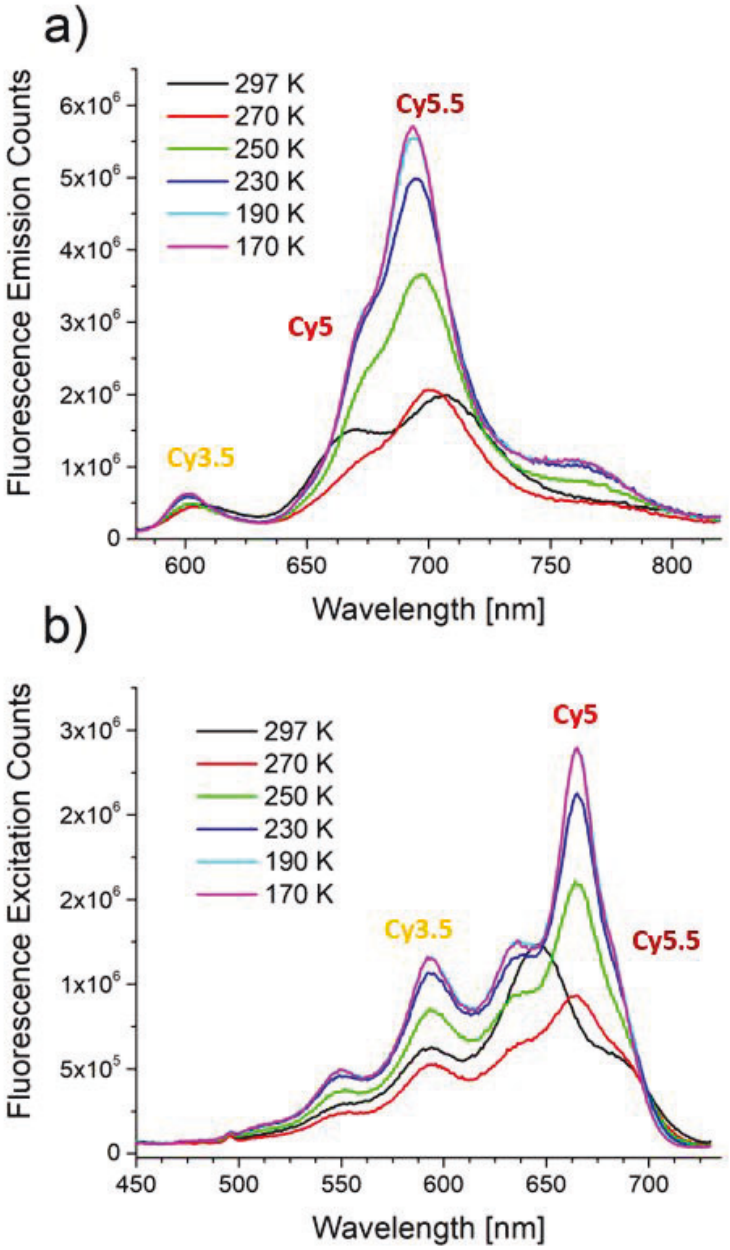

170 K. At 170 K, the two lowest excitonic transitions of $D0_{Cy5}$ in the fluorescence excitation spectrum can be resolved at 666 nm and 634 nm, indicating a Davydov splitting of about 760 cm^{-1}.

Figure 6. Temperature-dependent fluorescence spectra. a) Temperature-dependent fluorescence emission spectra of MPW2($D0_{Cy5}$) in Gly-PBS from 515 nm excitation. Approximate emission maxima for each dye indicated. b) Temperature-dependent fluorescence excitation spectra of MPW2($D0_{Cy5}$) in Gly-PBS for detection at 750 nm. Approximate excitation maxima for each dye is indicated.

$E_{ee,sens}$ at 170 K was estimated by extracting the Cy5.5 fluorescence band from the MPW2($D0_{Cy5}$) fluorescence emission spectrum using $C_{Cy3.5}$ and C_{Cy5} fluorescence emission spectra measured at 170 K, accounting for direct excitation, and estimating the fluorescence quantum yields of $C_{Cy3.5}$ and $C_{Cy5.5}$ at 170 K (**Figures S14 a-d**). Using this procedure, we estimate $E_{ee,sens}$ at 170 K to be 0.75 ± 0.10. This represents approximately a 7-fold increase in EQE compared to $E_{ee,sens}$ at room temperature in PBS. The large increase is consistent with suppressed non-radiative relaxation in 0 bp cyanine dimers at low temperature.[34, 67-69] The experimental value may be compared to the theoretical prediction of 92% for end-to-end EQE for each transfer step occurring in the limit of static isotropic dyes. As in the case of MPW1($D0_{Cy3}$), a plausible explanation for the discrepancy between experimental and theoretical EQEs is related to constrained transition dipoles in unfavorable relative orientations for FRET.

As a final comment, we note that the predicted benefit of J-dimer donor compared to a monomer donor is rather modest for a single FRET step. However, in the SI (Section 10), we show theoretically that a substantial benefit can be obtained from arrays of J-dimer relays over arrays monomer relays in MPWs where energy transfer occurs by multi-step homoFRET.[70, 71] For example, for an array consisting of six relay units (Figure S15), the energy transfer from an array of ideal Cy3 J-dimers can be as much as a factor of 2 higher than from a corresponding array of ideal Cy3 monomers (SI, Section 10). This theoretical result underlies the potential benefit of using an extended J-dimer relay for efficient long-range FRET.

SUMMARY AND CONCLUSIONS

In this work, we experimentally characterized the energy transfer properties of DNA-templated MPWs that use J-like Cy3 and Cy5 dimers as relay units between a dye monomer donor and a dye monomer acceptor. We also performed MD simulations to provide insight into how dye orientation affected the EQE. While we did not observe that the dimer relays produce greater EQEs than cyanine monomer relays, we were still able to draw useful conclusions from the study. One conclusion is that while strong excitonic coupling in J-like Cy3 and Cy5 dimers leads to strong excited state quenching of the dimer, the quenching could be mitigated by using a viscous solvent

or by moderate sample cooling. These approaches led to substantial increases in the EQE in both MPWs and especially so for the more strongly coupled Cy5 dimer, which exhibited a ~7-fold increase in EQE when measured at 170 K. Furthermore, because the excited state quenching correlates with cyanine dye flexibility about the methine bridge, one could attempt to add rigidity to the nano-environment through DNA crowding. For example, DNA origami structures and DNA crystal scaffolds have been shown to constrain the rotational flexibility of Cy3,[58, 72] which is supported by increases in the Cy3 excited state lifetime and fluorescence anisotropy time. We speculate that the increased rigidity of DNA origami and DNA crystal scaffolds would substantially increase the excited state lifetimes of strongly coupled Cy3 and Cy5 dimers at room temperature. Recently, the Mathur and Veneziano labs demonstrated the use of asymmetric polymerase chain reaction to obtain precisely modified DNA origami template sequences at high yield.[73] This is a key factor, as only modifying DNA origami staple strands limits the capability to create closely spaced dye dimers. In addition to providing extra rigidity, DNA origami also provides a high density of dye attachment sites in two- and three dimensions and therefore offers high flexibility to design dye aggregates for efficient energy transfer.[58]

A second conclusion is that there is room to improve energy transfer through the J-like dimer by optimizing dye orientation for larger FRET rates. Because the Cy3 dimer is oblique, the oscillator strength is distributed between the J-like and H-like states. Realizing a dimer configuration that is closer to an ideal J-dimer would increase the collective emission dipole, which in turn would enhance the FRET rate to the acceptor dye. Even more important is the necessity to achieve a more favorable relative orientation between the dimer relay emission dipole and the terminal acceptor. These results emphasize the need to attain better control of dye orientation on DNA scaffolds, which is a challenging problem for the field of DNA nanotechnology. Current approaches include tuning the chemical structure of the dye molecule in order to control intermolecular interactions between closely spaced dyes,[74, 75] and tuning dye-DNA interactions through altering the properties of the local DNA scaffold to control the orientation covalently attached dye molecules.[28, 58-60, 76] We anticipate that these initial studies will inspire further efforts to improve the performance of DNA-templated dye aggregates for photonic applications.

ACKNOWLEDGMENTS

Research at the U.S. Naval Research Laboratory (NRL) was supported by NRL base funding, the NRL Institute for Nanoscience, and ONR award # N0001419WX01811. Research at Boise State

University, including data collection, analysis, and interpretation and manuscript preparation, was supported by the National Science Foundation (NSF) through the Integrated NSF Support Promoting Interdisciplinary Research and Education (INSPIRE) via award no. 1648655.

CONFLICT OF INTEREST

The Authors declare no conflict of interests.

SUPPORTING INFORMATION

The Supporting Information file includes dye structures; schematics and sequences of MPWs; analytical characterization of MPWs and control structures and reproducibility of optical spectra; additional absorption, CD and fluorescence spectra of MPWs and control structures; fluorescence decay measurements and fits; energy transfer quantum yields from donor fluorescence loss measurements; additional results from MD simulations including representative MD snapshots dye-DNA structures; estimations of EQEs, and fluctuations in κ^2 and R; estimation of EQE from cryogenic fluorescence measurements; simulation of homoFRET via random walks on ideal MPWs.

REFERENCES

(1) Scholes, G. D.; Fleming, G. R.; Olaya-Castro, A.; van Grondelle, R. Lessons from nature about solar light harvesting. *Nature Chemistry* **2011**, *3* (10), 763-774, DOI: 10.1038/nchem.1145.

(2) Brixner, T.; Hildner, R.; Köhler, J.; Lambert, C.; Würthner, F. Exciton Transport in Molecular Aggregates – From Natural Antennas to Synthetic Chromophore Systems. *Advanced Energy Materials* **2017**, *7* (16), 1700236, DOI: 10.1002/aenm.201700236.

(3) Mathur, D.; Díaz, S. A.; Hildebrandt, N.; Pensack, R. D.; Yurke, B.; Biaggne, A.; Li, L.; Melinger, J. S.; Ancona, M. G.; Knowlton, W. B.; et al. Pursuing excitonic energy transfer with programmable DNA-based optical breadboards. *Chemical Society Reviews* **2023**, *52* (22), 7848-7948, DOI: 10.1039/D0CS00936A.

(4) Cheng, Y.-J.; Yang, S.-H.; Hsu, C.-S. Synthesis of Conjugated Polymers for Organic Solar Cell Applications. *Chemical Reviews* **2009**, *109* (11), 5868-5923, DOI: 10.1021/cr900182s.

(5) Menke, S. M.; Holmes, R. J. Exciton diffusion in organic photovoltaic cells. *Energy & Environmental Science* **2014**, *7* (2), 499-512, DOI: 10.1039/C3EE42444H.

(6) Zadran, S.; Standley, S.; Wong, K.; Otiniano, E.; Amighi, A.; Baudry, M. Fluorescence resonance energy transfer (FRET)-based biosensors: visualizing cellular dynamics and

bioenergetics. *Appl Microbiol Biotechnol* **2012**, *96* (4), 895-902, DOI: 10.1007/s00253-012-4449-6.

(7) Yurke, B.; Kuang, W. Passive linear nanoscale optical and molecular electronics device synthesis from nanoparticles. *Physical Review A* **2010**, *81* (3), 033814, DOI: 10.1103/PhysRevA.81.033814.

(8) Fassioli, F.; Oblinsky, D. G.; Scholes, G. D. Designs for molecular circuits that use electronic coherence. *Faraday Discussions* **2013**, *163* (0), 341-351, DOI: 10.1039/C3FD00009E.

(9) Sawaya, N. P. D.; Rappoport, D.; Tabor, D. P.; Aspuru-Guzik, A. Excitonics: A Set of Gates for Molecular Exciton Processing and Signaling. *ACS Nano* **2018**, *12* (7), 6410-6420, DOI: 10.1021/acsnano.8b00584.

(10) Castellanos, M. A.; Dodin, A.; Willard, A. P. On the design of molecular excitonic circuits for quantum computing: the universal quantum gates. *Physical Chemistry Chemical Physics* **2020**, *22* (5), 3048-3057, DOI: 10.1039/C9CP05625D.

(11) Kellis, D. L.; Sarter, C.; Cannon, B. L.; Davis, P. H.; Graugnard, E.; Lee, J.; Pensack, R. D.; Kolmar, T.; Jäschke, A.; Yurke, B.; et al. An All-Optical Excitonic Switch Operated in the Liquid and Solid Phases. *ACS Nano* **2019**, *13* (3), 2986-2994, DOI: 10.1021/acsnano.8b07504.

(12) Cannon, B. L.; Kellis, D. L.; Davis, P. H.; Lee, J.; Kuang, W.; Hughes, W. L.; Graugnard, E.; Yurke, B.; Knowlton, W. B. Excitonic AND Logic Gates on DNA Brick Nanobreadboards. *ACS Photonics* **2015**, *2* (3), 398-404 DOI: 10.1021/ph500444d.

(13) Santangelo, P. J.; Nix, B.; Tsourkas, A.; Bao, G. Dual FRET molecular beacons for mRNA detection in living cells. *Nucleic Acids Res* **2004**, *32* (6), e57, DOI: 10.1093/nar/gnh062 .

(14) Kolpashchikov, D. M. An elegant biosensor molecular beacon probe: challenges and recent solutions. *Scientifica (Cairo)* **2012**, *2012*, 928783, DOI: 10.6064/2012/928783.

(15) Thomas, S. W.; Joly, G. D.; Swager, T. M. Chemical Sensors Based on Amplifying Fluorescent Conjugated Polymers. *Chemical Reviews* **2007**, *107* (4), 1339-1386, DOI: 10.1021/cr0501339.

(16) Gilat, S. L.; Adronov, A.; Fréchet, J. M. J. Light Harvesting and Energy Transfer in Novel Convergently Constructed Dendrimers. *Angewandte Chemie International Edition* **1999**, *38* (10), 1422-1427, DOI:10.1002/(SICI)1521-3773(19990517)38:10<1422::AID-ANIE1422>3.0.CO;2-V.

(17) Devadoss, C.; Bharathi, P.; Moore, J. S. Energy Transfer in Dendritic Macromolecules: Molecular Size Effects and the Role of an Energy Gradient. *Journal of the American Chemical Society* **1996**, *118* (40), 9635-9644, DOI: 10.1021/ja961418t.

(18) Kleiman, V. D.; Melinger, J. S.; McMorrow, D. Ultrafast Dynamics of Electronic Excitations in a Light-Harvesting Phenylacetylene Dendrimer. *The Journal of Physical Chemistry B* **2001**, *105* (24), 5595-5598, DOI: 10.1021/jp010208m.

(19) Heilemann, M.; Tinnefeld, P.; Sanchez Mosteiro, G.; Garcia Parajo, M.; Van Hulst, N. F.; Sauer, M. Multistep Energy Transfer in Single Molecular Photonic Wires. *Journal of the American Chemical Society* **2004**, *126* (21), 6514-6515, DOI: 10.1021/ja049351u.

(20) Díaz, S. A.; Buckhout-White, S.; Ancona, M. G.; Spillmann, C. M.; Goldman, E. R.; Melinger, J. S.; Medintz, I. L. Extending DNA-Based Molecular Photonic Wires with Homogeneous Förster Resonance Energy Transfer. *Advanced Optical Materials* **2016**, *4* (3), 399-412, DOI: 10.1002/adom.201500554.

(21) Boulais, É.; Sawaya, N. P. D.; Veneziano, R.; Andreoni, A.; Banal, J. L.; Kondo, T.; Mandal, S.; Lin, S.; Schlau-Cohen, G. S.; Woodbury, N. W.; et al. Programmed coherent coupling in a synthetic DNA-based excitonic circuit. *Nature Materials* **2018**, *17* (2), 159-166, DOI: 10.1038/nmat5033.

(22) Zhou, X.; Mandal, S.; Jiang, S.; Lin, S.; Yang, J.; Liu, Y.; Whitten, D. G.; Woodbury, N. W.; Yan, H. Efficient Long-Range, Directional Energy Transfer through DNA-Templated Dye Aggregates. *J Am Chem Soc* **2019**, *141* (21), 8473-8481, DOI: 10.1021/jacs.9b01548.

(23) Hannah, K. C.; Armitage, B. A. DNA-Templated Assembly of Helical Cyanine Dye Aggregates: A Supramolecular Chain Polymerization. *Accounts of Chemical Research* **2004**, *37* (11), 845-853, DOI: 10.1021/ar030257c.

(24) Strümpfer, J.; Şener, M.; Schulten, K. How Quantum Coherence Assists Photosynthetic Light-Harvesting. *The Journal of Physical Chemistry Letters* **2012**, *3* (4), 536-542, DOI: 10.1021/jz201459c.

(25) Scholes, G. D. Designing light-harvesting antenna systems based on superradiant molecular aggregates. *Chemical Physics* **2002**, *275* (1), 373-386, DOI: 10.1016/S0301-0104(01)00533-X.

(26) Muñoz-Losa, A.; Curutchet, C.; Krueger, B. P.; Hartsell, L. R.; Mennucci, B. Fretting about FRET: failure of the ideal dipole approximation. *Biophysical journal* **2009**, *96* (12), 4779-4788, DOI: 10.1016/j.bpj.2009.03.052 PubMed.

(27) Kringle, L.; Sawaya, N. P. D.; Widom, J.; Adams, C.; Raymer, M. G.; Aspuru-Guzik, A.; Marcus, A. H. Temperature-dependent conformations of exciton-coupled Cy3 dimers in double-stranded DNA. *The Journal of Chemical Physics* **2018**, *148* (8), 085101, DOI: 10.1063/1.5020084.

(28) Hart, S. M.; Chen, W. J.; Banal, J. L.; Bricker, W. P.; Dodin, A.; Markova, L.; Vyborna, Y.; Willard, A. P.; Häner, R.; Bathe, M.; et al. Engineering couplings for exciton transport using synthetic DNA scaffolds. *Chem* **2021**, *7* (3), 752-773, DOI: 10.1016/j.chempr.2020.12.020.

(29) Cannon, B. L.; Patten, L. K.; Kellis, D. L.; Davis, P. H.; Lee, J.; Graugnard, E.; Yurke, B.; Knowlton, W. B. Large Davydov Splitting and Strong Fluorescence Suppression: An Investigation of Exciton Delocalization in DNA-Templated Holliday Junction Dye Aggregates. *The Journal of Physical Chemistry A* **2018**, *122* (8), 2086-2095, DOI: 10.1021/acs.jpca.7b12668.

(30) Chowdhury, A. U.; Díaz, S. A.; Huff, J. S.; Barclay, M. S.; Chiriboga, M.; Ellis, G. A.; Mathur, D.; Patten, L. K.; Sup, A.; Hallstrom, N.; et al. Tuning between Quenching and Energy Transfer in DNA-Templated Heterodimer Aggregates. *The Journal of Physical Chemistry Letters* **2022**, *13* (12), 2782-2791, DOI: 10.1021/acs.jpclett.2c00017.

(31) Markova, L. I.; Malinovskii, V. L.; Patsenker, L. D.; Häner, R. J- vs. H-type assembly: pentamethine cyanine (Cy5) as a near-IR chiroptical reporter. *Chemical Communications* **2013**, *49* (46), 5298-5300, DOI: 10.1039/C3CC42103A.

(32) Cunningham, P. D.; Kim, Y. C.; Díaz, S. A.; Buckhout-White, S.; Mathur, D.; Medintz, I. L.; Melinger, J. S. Optical Properties of Vibronically Coupled Cy3 Dimers on DNA Scaffolds. *The Journal of Physical Chemistry B* **2018**, *122* (19), 5020-5029, DOI: 10.1021/acs.jpcb.8b02134.

(33) Nicoli, F.; Roos, M. K.; Hemmig, E. A.; Di Antonio, M.; de Vivie-Riedle, R.; Liedl, T. Proximity-Induced H-Aggregation of Cyanine Dyes on DNA-Duplexes. *The Journal of Physical Chemistry A* **2016**, *120* (50), 9941-9947, DOI: 10.1021/acs.jpca.6b10939.

(34) Rolczynski, B. S.; Díaz, S. A.; Kim, Y. C.; Medintz, I. L.; Cunningham, P. D.; Melinger, J. S. Understanding Disorder, Vibronic Structure, and Delocalization in Electronically Coupled Dimers on DNA Duplexes. *The Journal of Physical Chemistry A* **2021**, *125* (44), 9632-9644, DOI: 10.1021/acs.jpca.1c07205.

(35) Cannon, B. L.; Kellis, D. L.; Patten, L. K.; Davis, P. H.; Lee, J.; Graugnard, E.; Yurke, B.; Knowlton, W. B. Coherent Exciton Delocalization in a Two-State DNA-Templated Dye

Aggregate System. *The Journal of Physical Chemistry A* **2017**, *121* (37), 6905-6916, DOI: 10.1021/acs.jpca.7b04344.

(36) Sanborn, M. E.; Connolly, B. K.; Gurunathan, K.; Levitus, M. Fluorescence Properties and Photophysics of the Sulfoindocyanine Cy3 Linked Covalently to DNA. *The Journal of Physical Chemistry B* **2007**, *111* (37), 11064-11074, DOI: 10.1021/jp072912u.

(37) Hammond, P. R. Self-absorption of molecular fluorescence, the design of equipment for measurement of fluorescence decay, and the decay times of some laser dyesa). *The Journal of Chemical Physics* **1979**, *70* (8), 3884-3894, DOI: 10.1063/1.437940.

(38) Zhang, X.-F.; Zhang, J.; Liu, L. Fluorescence Properties of Twenty Fluorescein Derivatives: Lifetime, Quantum Yield, Absorption and Emission Spectra. *Journal of Fluorescence* **2014**, *24* (3), 819-826, DOI: 10.1007/s10895-014-1356-5.

(39) Arbeloa, F. L.; Ojeda, P. R.; Arbeloa, I. L. Flourescence self-quenching of the molecular forms of Rhodamine B in aqueous and ethanolic solutions. *Journal of Luminescence* **1989**, *44* (1), 105-112, DOI: 10.1016/0022-2313(89)90027-6.

(40) Birge, R. Kodak laser dyes. *Kodak publication JJ-169* **1987**.

(41) Alessi, A.; Salvalaggio, M.; Ruzzon, G. Rhodamine 800 as reference substance for fluorescence quantum yield measurements in deep red emission range. *Journal of Luminescence* **2013**, *134*, 385-389, DOI: 10.1016/j.jlumin.2012.08.017.

(42) Hannestad, J. K.; Sandin, P.; Albinsson, B. Self-Assembled DNA Photonic Wire for Long-Range Energy Transfer. *Journal of the American Chemical Society* **2008**, *130* (47), 15889-15895, DOI: 10.1021/ja803407t.

(43) Boeneman, K.; Prasuhn, D. E.; Blanco-Canosa, J. B.; Dawson, P. E.; Melinger, J. S.; Ancona, M.; Stewart, M. H.; Susumu, K.; Huston, A.; Medintz, I. L. Self-assembled quantum dot-sensitized multivalent DNA photonic wires. *J Am Chem Soc* **2010**, *132* (51), 18177-18190, DOI: 10.1021/ja106465x From NLM.

(44) Watrob, H. M.; Pan, C.-P.; Barkley, M. D. Two-Step FRET as a Structural Tool. *Journal of the American Chemical Society* **2003**, *125* (24), 7336-7343, DOI: 10.1021/ja034564p.

(45) Moroz, P.; Klein, W. P.; Akers, K.; Vore, A.; Kholmicheva, N.; Razgoniaeva, N.; Khon, D.; Díaz, S. A.; Medintz, I. L.; Zamkov, M. Lifting the Spectral Crosstalk in Multifluorophore Assemblies. *The Journal of Physical Chemistry C* **2017**, *121* (47), 26226-26232, DOI: 10.1021/acs.jpcc.7b09396.

(46) Taniguchi, M.; Du, H.; Lindsey, J. S. PhotochemCAD 3: Diverse Modules for Photophysical Calculations with Multiple Spectral Databases. *Photochemistry and Photobiology* **2018**, *94* (2), 277-289, DOI: 10.1111/php.12862.

(47) Van Der Spoel, D.; Lindahl, E.; Hess, B.; Groenhof, G.; Mark, A. E.; Berendsen, H. J. C. GROMACS: Fast, flexible, and free. *Journal of Computational Chemistry* **2005**, *26* (16), 1701-1718, DOI: 10.1002/jcc.20291.

(48) Hornak, V.; Abel, R.; Okur, A.; Strockbine, B.; Roitberg, A.; Simmerling, C. Comparison of multiple Amber force fields and development of improved protein backbone parameters. *Proteins: Structure, Function, and Bioinformatics* **2006**, *65* (3), 712-725, DOI: 10.1002/prot.21123.

(49) Wang, J.; Wolf, R. M.; Caldwell, J. W.; Kollman, P. A.; Case, D. A. Development and testing of a general amber force field. *Journal of Computational Chemistry* **2004**, *25* (9), 1157-1174, DOI: 10.1002/jcc.20035.

(50) Hess, B.; Bekker, H.; Berendsen, H. J. C.; Fraaije, J. G. E. M. LINCS: A linear constraint solver for molecular simulations. *Journal of Computational Chemistry* **1997**, *18* (12), 1463-1472, DOI: 10.1002/(SICI)1096-987X(199709)18:12<1463::AID-JCC4>3.0.CO;2-H.

(51) Pettersen, E. F.; Goddard, T. D.; Huang, C. C.; Couch, G. S.; Greenblatt, D. M.; Meng, E. C.; Ferrin, T. E. UCSF Chimera--a visualization system for exploratory research and analysis. *J Comput Chem* **2004**, *25* (13), 1605-1612, DOI: 10.1002/jcc.20084.

(52) Bussi, G.; Donadio, D.; Parrinello, M. Canonical sampling through velocity rescaling. *The Journal of Chemical Physics* **2007**, *126* (1), 014101, DOI: 10.1063/1.2408420.

(53) Parrinello, M.; Rahman, A. Polymorphic transitions in single crystals: A new molecular dynamics method. *Journal of Applied Physics* **1981**, *52* (12), 7182-7190, DOI: 10.1063/1.328693.

(54) Díaz, S. A.; Pascual, G.; Patten, L. K.; Roy, S. K.; Meares, A.; Chiriboga, M.; Susumu, K.; Knowlton, W. B.; Cunningham, P. D.; Mathur, D.; et al. Towards control of excitonic coupling in DNA-templated Cy5 aggregates: the principal role of chemical substituent hydrophobicity and steric interactions. *Nanoscale* **2023**, DOI: 10.1039/D2NR05544A.

(55) Iqbal, A.; Arslan, S.; Okumus, B.; Wilson, T. J.; Giraud, G.; Norman, D. G.; Ha, T.; Lilley, D. M. J. Orientation dependence in fluorescent energy transfer between Cy3 and Cy5 terminally attached to double-stranded nucleic acids. *Proceedings of the National Academy of Sciences* **2008**, *105* (32), 11176-11181, DOI: doi:10.1073/pnas.0801707105.

(56) Vogel, S. S.; van der Meer, B. W.; Blank, P. S. Estimating the distance separating fluorescent protein FRET pairs. *Methods* **2014**, *66* (2), 131-138, DOI: 10.1016/j.ymeth.2013.06.021.

(57) Melinger, J. S.; Khachatrian, A.; Ancona, M. G.; Buckhout-White, S.; Goldman, E. R.; Spillmann, C. M.; Medintz, I. L.; Cunningham, P. D. FRET from Multiple Pathways in Fluorophore-Labeled DNA. *ACS Photonics* **2016**, *3* (4), 659-669, DOI: 10.1021/acsphotonics.6b00006.

(58) Mathur, D.; Kim, Y. C.; Díaz, S. A.; Cunningham, P. D.; Rolczynski, B. S.; Ancona, M. G.; Medintz, I. L.; Melinger, J. S. Can a DNA Origami Structure Constrain the Position and Orientation of an Attached Dye Molecule? *The Journal of Physical Chemistry C* **2021**, *125* (2), 1509-1522, DOI: 10.1021/acs.jpcc.0c09258.

(59) Cervantes-Salguero, K.; Biaggne, A.; Youngsman, J. M.; Ward, B. M.; Kim, Y. C.; Li, L.; Hall, J. A.; Knowlton, W. B.; Graugnard, E.; Kuang, W. Strategies for Controlling the Spatial Orientation of Single Molecules Tethered on DNA Origami Templates Physisorbed on Glass Substrates: Intercalation and Stretching. *International Journal of Molecular Sciences* **2022**, *23* (14), 7690, DOI:10.3390/ijms2314769

(60) Hübner, K.; Joshi, H.; Aksimentiev, A.; Stefani, F. D.; Tinnefeld, P.; Acuna, G. P. Determining the In-Plane Orientation and Binding Mode of Single Fluorescent Dyes in DNA Origami Structures. *Acs Nano* **2021**, *15* (3), 5109-5117, DOI: 10.1021/acsnano.0c10259.

(61) Biaggne, A.; Knowlton, W. B.; Yurke, B.; Lee, J.; Li, L. Substituent Effects on the Solubility and Electronic Properties of the Cyanine Dye Cy5: Density Functional and Time-Dependent Density Functional Theory Calculations. *Molecules* **2021**, *26* (3), 524, DOI: 10.3390/molecules26030524

(62) Kistler, K. A.; Pochas, C. M.; Yamagata, H.; Matsika, S.; Spano, F. C. Absorption, Circular Dichroism, and Photoluminescence in Perylene Diimide Bichromophores: Polarization-Dependent H- and J-Aggregate Behavior. *The Journal of Physical Chemistry B* **2012**, *116* (1), 77-86, DOI: 10.1021/jp208794t.

(63) Barclay, M. S.; Wilson, C. K.; Roy, S. K.; Mass, O. A.; Obukhova, O. M.; Svoiakov, R. P.; Tatarets, A. L.; Chowdhury, A. U.; Huff, J. S.; Turner, D. B.; et al. Oblique Packing and Tunable Excitonic Coupling in DNA-Templated Squaraine Rotaxane Dimer Aggregates. *ChemPhotoChem* **2022**, *6* (7), e202200039, DOI: 10.1002/cptc.202200039.

(64) Muenter, A. A.; Brumbaugh, D. V.; Apolito, J.; Horn, L. A.; Spano, F. C.; Mukamel, S. Size dependence of excited-state dynamics for J-aggregates at silver bromide interfaces. *The Journal of Physical Chemistry* **1992**, *96* (7), 2783-2790, DOI: 10.1021/j100186a002.

(65) Yakovchuk, P.; Protozanova, E.; Frank-Kamenetskii, M. D. Base-stacking and base-pairing contributions into thermal stability of the DNA double helix. *Nucleic Acids Research* **2006**, *34* (2), 564-574, DOI: 10.1093/nar/gkj454.

(66) Huff, J. S.; Davis, P. H.; Christy, A.; Kellis, D. L.; Kandadai, N.; Toa, Z. S. D.; Scholes, G. D.; Yurke, B.; Knowlton, W. B.; Pensack, R. D. DNA-Templated Aggregates of Strongly Coupled Cyanine Dyes: Nonradiative Decay Governs Exciton Lifetimes. *The Journal of Physical Chemistry Letters* **2019**, *10* (10), 2386-2392, DOI: 10.1021/acs.jpclett.9b00404.

(67) Cunningham, P. D.; Diaz, S. A.; Yurke, B.; Medintz, I. L.; Melinger, J. S. Delocalized Two-Exciton States in DNA Scaffolded Cyanine Dimers. *Journal of Physical Chemistry B* **2020**, *124* (37), 8042-8049, DOI: 10.1021/acs.jpcb.0c06732.

(68) Mazuski, R. J.; Diaz, S. A.; Wood, R. E.; Lloyd, L. T.; Klein, W. P.; Mathur, D.; Melinger, J. S.; Engel, G. S.; Medintz, I. L. Ultrafast Excitation Transfer in Cy5 DNA Photonic Wires Displays Dye Conjugation and Excitation Energy Dependency. *Journal of Physical Chemistry Letters* **2020**, *11* (10), 4163-4172, DOI: 10.1021/acs.jpclett.0c01020.

(69) Díaz, S. A.; Oliver, S. M.; Hastman, D. A.; Medintz, I. L.; Vora, P. M. Increased Transfer Efficiency from Molecular Photonic Wires on Solid Substrates and Cryogenic Conditions. *The Journal of Physical Chemistry Letters* **2018**, *9* (13), 3654-3659, DOI: 10.1021/acs.jpclett.8b00931.

(70) Klein, W. P.; Rolczynski, B. S.; Oliver, S. M.; Zadegan, R.; Buckhout-White, S.; Ancona, M. G.; Cunningham, P. D.; Melinger, J. S.; Vora, P. M.; Kuang, W.; et al. DNA Origami Chromophore Scaffold Exploiting HomoFRET Energy Transport to Create Molecular Photonic Wires. *Acs Applied Nano Materials* **2020**, *3* (4), 3323-3336, DOI: 10.1021/acsanm.0c00038.

(71) Klein, W. P.; Díaz, S. A.; Buckhout-White, S.; Melinger, J. S.; Cunningham, P. D.; Goldman, E. R.; Ancona, M. G.; Kuang, W.; Medintz, I. L. Utilizing HomoFRET to Extend DNA-Scaffolded Photonic Networks and Increase Light-Harvesting Capability. *Advanced Optical Materials* **2018**, *6* (1), 1700679, DOI: 10.1002/adom.201700679.

(72) Melinger, J. S.; Sha, R.; Mao, C.; Seeman, N. C.; Ancona, M. G. Fluorescence and Energy Transfer in Dye-Labeled DNA Crystals. *The Journal of Physical Chemistry B* **2016**, *120* (48), 12287-12292, DOI: 10.1021/acs.jpcb.6b09385.

(73) Oktay, E.; Bush, J.; Vargas, M.; Scarton, D. V.; O'Shea, B.; Hartman, A.; Green, C. M.; Neyra, K.; Gomes, C. M.; Medintz, I. L.; et al. Customized Scaffolds for Direct Assembly of Functionalized DNA Origami. *ACS Applied Materials & Interfaces* **2023**, *15* (23), 27759-27773, DOI: 10.1021/acsami.3c05690.
(74) Meares, A.; Susumu, K.; Mathur, D.; Lee, S. H.; Mass, O. A.; Lee, J.; Pensack, R. D.; Yurke, B.; Knowlton, W. B.; Melinger, J. S.; et al. Synthesis of Substituted Cy5 Phosphoramidite Derivatives and Their Incorporation into Oligonucleotides Using Automated DNA Synthesis. *ACS Omega* **2022**, *7* (13), 11002-11016, DOI: 10.1021/acsomega.1c06921.
(75) Mass, O. A.; Wilson, C. K.; Barcenas, G.; Terpetschnig, E. A.; Obukhova, O. M.; Kolosova, O. S.; Tatarets, A. L.; Li, L.; Yurke, B.; Knowlton, W. B.; et al. Influence of Hydrophobicity on Excitonic Coupling in DNA-Templated Indolenine Squaraine Dye Aggregates. *The Journal of Physical Chemistry C* **2022**, *126* (7), 3475-3488, DOI: 10.1021/acs.jpcc.1c08981.
(76) Adamczyk, A. K.; Huijben, T. A. P. M.; Sison, M.; Di Luca, A.; Chiarelli, G.; Vanni, S.; Brasselet, S.; Mortensen, K. I.; Stefani, F. D.; Pilo-Pais, M.; et al. DNA Self-Assembly of Single Molecules with Deterministic Position and Orientation. *ACS Nano* **2022**, *16* (10), 16924-16931, DOI: 10.1021/acsnano.2c06936.

TOC GRAPHIC.

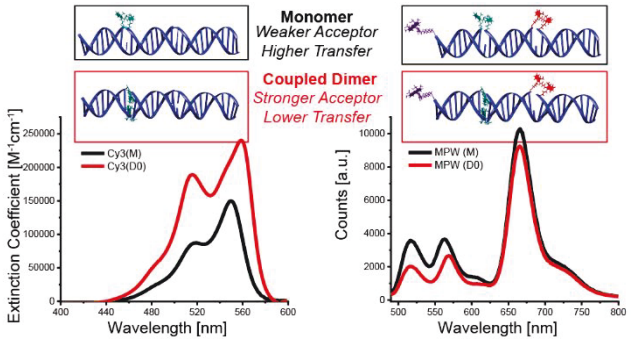

Schematic depicting end-to-end energy transfer in DNA templated molecular photonic wires through either a monomer intermediate or an excitonic Cy3 dimer intermediate.